~~Assimilation sensitivity~~ Sensitivity of ~~satellite-derived surface melt into~~ the Regional Climate Model MAR~~: case study over~~ ’s snowpack to the assimilation parametrization of satellite-derived wet-snow masks on the Antarctic Peninsula

Thomas Dethinne[1,2], Quentin Glaude[1,3], Ghislain Picard[4], Christoph Kittel[5], Anne Orban[3], and Xavier Fettweis[1]

[1]University of Liège, SPHERES research unit, Laboratory of Climatology, Liège, Belgium
[2]University of Liège, SPHERES research unit, Earth Observation and Ecosystem Monitoring laboratory, Liège, Belgium
[3]University of Liège, Centre Spatial de Liège, Signal Processing Laboratory, Liège, Belgium
[4]Institut des Géosciences de l’Environnement (IGE), Université Grenoble Alpes/CNRS/UMR 5001, Grenoble, France
[5]Institut des Géosciences de l’Environnement (IGE), Université Grenoble Alpes/CNRS/IRD/G-INP, Grenoble, France

Correspondence: Thomas Dethinne (tdethinne@uliege.be)

Abstract. ~~The study of the recent variability and the future projections of the poles’ climate currently relies on polar-oriented Regional Climate Models~~ This paper discusses the use of regional climate models (RCMs) ~~. However, RCMs are subject to biases and systematic errors that impact the results of their simulations. Remote Sensing~~ and remote sensing (RS) data ~~can help to reduce these ambiguities by providing indirect observations to the modeled estimates. Using the behavior of radiofrequency signals with regard to the presence of water in a snowpack, passive and active microwave instruments such as AMSR2, ASCAT, and Sentinel-1 are used to detect melt at the surface of the snowpack~~to study climate change in remote regions such as the polar regions. RCMs can simulate how certain climate variables, such as surface melt, runoff, and snowfall, are likely to change in response to different climate scenarios, but they are subject to biases and errors. RS data can assist in reducing and quantifying the uncertainties of the model by providing indirect observations of the modeled variables upon the present climate. In this ~~paper~~work, we investigate the sensitivity of the RCM ~~“~~"Modèle Atmosphérique Régional~~”~~ " (MAR) to the ~~assimilation of surface melt~~ parameters of the assimilation of wet snow occurrence estimated by RS datasets. The assimilation is performed by nudging the MAR snowpack temperature to match the ~~observed melt state~~ presence of liquid water observed by satellite. The sensitivity is tested by modifying parameters of the assimilation~~: (i)~~ , such as the depth to which the MAR snowpack is warmed up or cooled down ~~(corresponding to the penetration depth of the satellites) to match with satellite, and (ii)~~ to match with the satellite based wet-snow extent, the quantity of water required into the snowpack to qualify a MAR pixel as ~~melting or not , and (iii)by assimilating multiple~~ wet or not (0.1 or 0.2% of the snowpack mass being water), and assimilating different RS datasets. The data assimilation is performed over the Antarctic Peninsula ~~for~~ over the 2019-2021 period. The results show an increase in ~~the melt production~~ surface melt (+66.7% on average, or +95 Gt) going along with a small decrease in surface mass balance (SMB) (-4.5% on average, or -20 Gt) for the 2019-2020 melt season. The model is sensitive to the ~~three parameters tested but with different~~ tested parameters, albeit with varying orders of magnitude. The ~~sensitivity to the assimilated dataset~~

is reduced by using multiple datasets during the assimilation and discarding the remote observations that are not coherent. For the other two parameters, the penetration assimilation depth has more impact on the assimilation resulting surface melt than the quantity of liquid water used as melt threshold. The first one is especially sensitive for the sensors with a shorter penetration depth. In the first centimeters, a densification due to a refreeze can impact the melt production and cause an overestimation of the melt production. For the second threshold, the impact is more important on the number of melt days rather than the melt production itself. content (LWC) required in the snowpack due to strong refreeze occurring in the top layers of the snowpack. The values tested for the quantity of liquid water LWC required into the snowpack to qualify a MAR pixel as melting or not (0.1 or 0.2 of the snowpack mass being water) wet or not are lower than during typical melt days (~approximately 1.2%) and impact results mainly at the beginning and the end of the melt periodwhen lower values are reached. Such an melting period. The assimilation will allow an uncertainty estimation of MAR 's melt production , as well as identifying potential issues at the snowpack surface processes. melt production and identify potential issues in the near-surface snowpack modeled processes. This paves the way for improving models to achieve more accurate simulations of the future.

1 Introduction

The polar ice sheets contain more More than two-thirds of the planet's freshwater (Church et al., 2013). If melted entirely, the Antarctic ice sheet Earth's freshwater is held in the polar ice sheets (Church et al., 2013), with the majority of it trapped as ice on the ground at the south pole, forming the Antarctic Ice Sheet (AIS)would cause an elevation of the sea level of . According to Fretwell et al. (2013), if all the ice in the AIS was to melt, it would result in a sea-level rise of 56 (Fretwell et al., 2013). As for nowmeters. Currently, the AIS is mainly losing mass from primarily losing mass due to grounded ice flowing into the ocean. There, the ice is lost mainly through a combination of basal melting and calving (The IMBIE Team, 2018; Rignot et al., 2019; Adusumilli et . However, surface melting is becoming an increasing concern with climate change (Trusel et al., 2015; Bell et al., 2018; Gilbert and Kittel, . Over (The IMBIE Team, 2018; Rignot et al., 2019; Adusumilli et al., 2020).

However, the surface melt production on the ice sheet is important for several reasons. Even moderate surface melt over the ice shelves, the floating boundaries of the ice sheet, the surface melt is known is thought to weaken the structure of the shelf and can cause shelf structure and to cause ponding and hydrofracturing, leading to even more mass loss (Scambos et al., 2003; Pollard et al., 201 . The thinning of the ice shelves also has consequences on the ice flow of the AIS. Although the ice shelves are smaller than the ice sheet, they exercise substantial mass loss (Scambos et al., 2003; Lai et al., 2020) and, surface melting is becoming a growing concern as it is taught to increase greatly with climate change (Trusel et al., 2015; Bell et al., 2018; Gilbert and Kittel, 2021) . Ice shelves exert a buttressing effect on the upstream ice flow, controlling the quantity of ice reaching regulating the amount of ice that reaches the surrounding ocean. Their thinning reduces that buttressing effect and consequently leads to an increase in mass loss (Favier and Pattyn, 2015; Paolo et al., 2015; Sun et al., 2020)As they thin from mass loss, this buttressing effect is reduced (Favier and Pattyn, 2015; Paolo et al., 2015), and AIS ice flow velocity is increased.

Climate models are nowadays one of the handiest tools to monitor the ice shelf evolution . For example , study polar climate evolution. Some of them also include the possibility to model the evolution of the snowpack. A notable example is MAR (for

"Modèle Atmosphérique Régional" in French)has been , a Regional Climate Model (RCM) especially developed to monitor the polar climate and the surface mass balance of both ice sheets. However, Regional Climate Models (RCMs)

Proper modeling of the surface melt is required to study both the conditions leading to the destabilization as hydrofracturing is impacted by the melting/snowfall ratio and by the snowpack capacity to retain and refreeze meltwater (Donat-Magnin et al., 2021; Gilbert , but also to study the evolution of the snowpack during strong melt events. Studying the snowpack ability to retain liquid water is crucial because the Antarctic snowpack could saturate, and stop absorbing surface meltwater in the future, as it is modeled currently over the Greenland ice sheet (Noël et al., 2017).

However, RCMs still have some limitations. Because of the forcing, or the physical assumptions, the models may contain significant uncertainties. Those may be reduced by using external datawith other independent sources of uncertainties to correct the modelat certain These uncertainties can be mitigated by employing external data, which is not already incorporated into the model, to improve its accuracy at specific points in space and/or time. This technique is known as "data assimilation" and is commonly applied in numerous fields where observations can be integrated into a model (Evensen, 2009; Bouchard et al., 2010; Navari et a (Evensen, 2009; Navari et al., 2018).

In this article, we sequentially assimilate satellite-derived surface melt occurrence over the Antarctic Peninsula (AP), West Antarctica, into the MAR model . Three major ice shelves are located over the AP: Larsen C, Georges VI, and Wilkins (Figure 1). These ice shelves undergo the most surface melt of the AIS, and their surface processes are also poorly understood, with a complex surface hydrology (Barrand et al., 2013; Datta et al., 2019; Johnson et al., 2020). Assimilation of data into the model is a crucial step in quantifying the uncertainties associated with the model output without assimilation. The assimilation process helps to identify areas and periods where the simulations are not consistent with the observations. This can help us better understand the underlying physical processes and their interactions. Accordingly, data assimilation provides a powerful tool for improving the reliability of models. In our case, it is an essential step in the process of model refinement, leading to improved predictions of future scenarios.

Location of the Antarctic Peninsula and the three studied ice shelves. The ice shelves are denoted by color outlines. Larsen C is outlined in purple, Georges VI in green, and Wilkins in red. Blue crosses indicate the position of the weather stations used for the evaluation of the model (Sect. 3).

The highly uneven topography of the area is challenging for the RCMs usually operating at kilometer-scale resolution. Localized phenomena like Foehn-effect induce melt a 10-kilometer spatial resolution. Phenomena depending on very local conditions such as melt induced by the Foehn effect can occur at a smaller spatial extent than the RCMs spatial resolution (Datta et al., 2019; Chuter et al., 2022; Wille et al., 2022)scale than the spatial resolution of RCMs and thus may be mitigated by the model (Datta et al., 2019; Chuter et al., 2022; Wille et al., 2022). However, high-resolution satellites can document these local events that could be missed by RMCs in case of localized or extreme events. In addition, using multiple satellites allows us to perform the assimilation over the whole studied zone every day

In this paper, we assimilate satellite-derived binary wet-snow masks (wet/non-wet) over the Antarctic Peninsula (AP), West Antarctica, into the MAR model for two melt seasons (2019-2020 and 2020-2021). As for now, assimilating remotely sensed Three major ice shelves are located over the AP: Larsen C, George VI, and Wilkins (Figure 1). These ice shelves undergo

the most surface melt of the AIS, and their surface processes are also poorly understood, with complex surface hydrology (Barrand et al., 2013; Datta et al., 2018; Johnson et al., 2020). Presently, assimilating remotely-sensed products in RCMs is a promising method to quantify the surface meltwater quantity in Antarctica. The scarcity of field observations and the complexity of the surface hydrology (Bell et al., 2018) make it ~~hard~~ difficult to evaluate and constrain models otherwise.

~~Modeling the surface melt production on the ice shelves is important for several reasons. One consequence of surface melting is the hydrofracturing, which destabilizes the ice shelves and therefore induces high mass loss (Donat-Magnin et al., 2021) . Hydrofracturing is impacted by the melting/snowfall ratio and by the snowpack capacity to retain and refreeze meltwater (Donat-Magnin et al., 2021; Gilbert and Kittel, 2021), a proper modeling of the surface melt is needed to study the conditions leading to the destabilization. In addition, proper modeling of the surface melt also makes possible the studyof the evolution of the snowpack during strong melt events. Studying the snowpack ability to retain liquid water is crucial because the Antarctic snowpack could saturate, and stop absorbing surface meltwater in the future, as observed currently over the Greenland ice sheet (Noël et al., 2017).~~

~~In this work, we present the results of the assimilation of~~ The assimilation algorithm performed in this paper is derived from the framework described in Kittel et al. (2022) where MAR near-surface snowpack is warmed up or cooled down to better match satellite-derived ~~melt into MAR and the methodology applied to test the sensitivity of the model to the assimilation. Experiments~~ wet-snow masks. In this study, experiments have been performed by varying the depth to which the snowpack temperature is changed (called the ~~penetration depth here after~~assimilation depth hereafter) to match satellites, the minimum liquid water quantity to consider the ~~model state as melting~~modeled snowpack state as wet, and the assimilated ~~melt product~~ wet-snow product to test the sensitivity of the model to the assimilation.

The satellite data, the model, and the assimilation are presented in Sect. 2. The validation of the model is described in Sect. 3. The results of the sensitivity tests when assimilating data into the model are discussed in Sect. 4. Finally, a general conclusion and discussions on the perspectives of the assimilation of remote sensing data in the MAR model are included in Sect. 5.

2 Methods and data

2.1 Satellite data

Depending on the context of the study, like the region of interest, the length of the simulation, or the spatial resolution, the use of ~~a~~ one specific satellite dataset over another for the assimilation can be useful~~as depending~~ . Reckoning on the sensor and acquisition times, ~~melt occurrence can be different (Husman et al., 2022). On the one hand, the passive~~ wet-snow occurrences derived from satellites can differ (Husman et al., 2022). Some sensors tend to have coarser resolution ~~than the active ones~~ and provide information with higher uncertainties in areas with complex topography ~~. Nonetheless, they provide~~ but provide longer time series of daily images with ~~melt~~ wet snow detection algorithms that have proven to be efficient ~~(Zwally and Fiegles, 1994; Torinesi et al., 2003; Colosio et al., 2021), and have been available for a longer time in the past~~(Zwally and Fieg . On the other hand, ~~active~~ other sensors have a better spatial resolution but may have a lower revisit time. The choice of the ~~assimilated~~ satellite dataset can thus influence the results of the assimilated model.

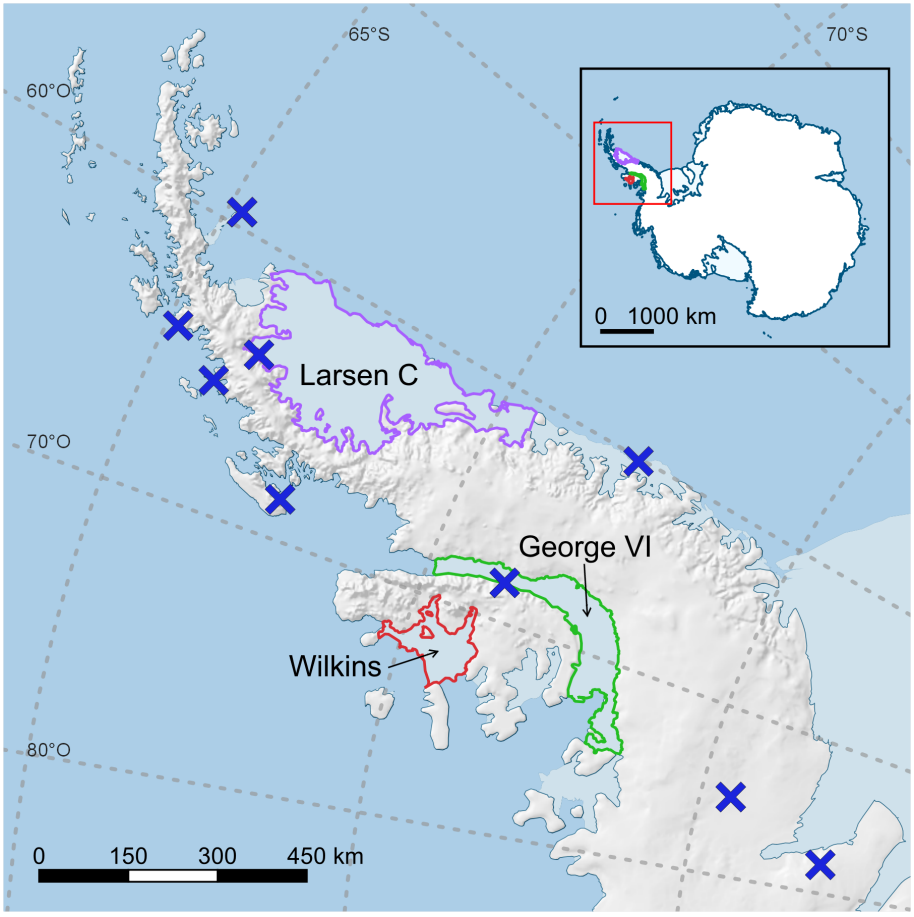

Figure 1. Locations of the Antarctic Peninsula and the three studied ice shelves. The ice shelves are denoted by color outlines. Larsen C is outlined in purple, George VI in green, and Wilkins in red. Blue crosses indicate the position of the weather stations used for the model's evaluation (Sect. 3).

~~The satellite data, the model and the assimilation are presented in Sect. 2. The validation of the model is described in Sect. 3. The results of the sensitivity tests when assimilating data into the model are discussed in Sect. 4. Finally, a general conclusion and discussions on the perspectives of the assimilation of remote sensing data in the MAR model are included in Sect. 5.~~

3 ~~Methods and data~~

2.1 ~~Satellite data~~

~~Three satellite datasets were used~~ We employed three satellite datasets (Table 1) to create the binary ~~melt masks~~ (dry/wet) wet-snow masks assimilated. The three ~~sensors operate in the microwaves (~~datasets are derived from sensors operating in

Table 1. Technical specifications of the remote sensing datasets employed for the assimilation. Datasets are referred to by the name in bold characters in the paper

Plateform	Sensor	Sensor type	Pixel size	Frequency (GHz)	Revisit time (days)	Reference
Sentinel-1 (S1)	C-SAR	Active	10-40m	5.405	6	ESA (2023)
Metop	**ASCAT**	Active	4.45km	5.255	1	EUMETSAT (2023)
GCOM-W1	**AMSR2**	Passive	10km	18.7	2	JAXA (2021)

the microwave spectrum (in the GHz ~~spectrum). Microwave radiometers~~ frequencies). Among them, one is called a "passive sensor" meaning the sensor records Earth's natural radiations, while the other two are classified as "active sensors" since they actively emit electromagnetic pulses to illuminate the area covered by the satellite. Microwave operating sensors are commonly used to map snow cover, sea ice, or the extension of ~~surface melt~~ wet snow over ice sheets ~~(Parkinson, 2001; Torinesi et al., 2003; Fettweis e~~ (Parkinson, 2001; Colosio et al., 2021). The signal is used to detect if the snowpack is wet ~~or not~~ as microwaves interact with water. The presence of liquid water in the snowpack induces a change ~~of~~ in its emissivity and absorptivity. This change leads to a change in the satellite ~~observables~~measurements, the backscattering coefficient σ_0 for active sensors and the brightness temperature for passive sensors ~~(Mätzler, 1987; Zwally and Fiegles, 1994; Johnson et al., 2022; Picard et al., 2022)~~(Zwally and Fiegles, 1994; Jol . In this study, the presence of ~~liquid water below~~ wet snow detected by satellites is interpreted as the presence of liquid water underneath or at the surface of the snowpack~~is interpreted as melting.~~

. Using microwaves also brings other advantages such as atmospheric transparency and ~~day/night acquisition capabilities~~day-and-night acquisitions. However, the ~~low resolution of radiometers~~ lower spatial resolution of passive microwave sensors (generally 10 to 50 km) compared to active sensors (generally 10 m to 5 km) is problematic to determine ~~small scale~~ small-scale melt extents (Datta et al., 2018). ~~The surface of one pixel is observed as homogeneous. With~~ Finally, with pixels of 100 km2 (for AMSR2 - See Table 1), a majority of the pixels are overlapping regions with different land cover or ~~topography (Johnson et al., 2020) . To override some limitations of the passive sensors, we also employed active sensors. In this case, the active sensors have a better spatial resolution than the passive ones but longer revisit time . In total, four melt masks are created from three sensors: one radiometer, one scatterometer and a radar.~~ surface height (Johnson et al., 2020).

2.0.1 Advanced Microwave Scanning Radiometer 2

In this study, we used ~~The~~ the Advanced Microwave Scanning Radiometer 2 (AMSR2) aboard the Global Change Observation Mission - Water "SHIZUKU" (GCOM-W1) retrieved from the Japan Aerospace Exploration Agency (JAXA) G-Portal ~~(JAXA, 2021)~~(JAXA, 2021). Thanks to the sun-synchronous orbit at an altitude of 700 km ~~,~~ and large swath, low-resolution daily observations of the polar regions are obtained. ~~The~~ We used the level-3 products ~~contain~~ containing the daily mean brightness temperature in horizontal polarization ~~at~~ in the 18.7 GHz channel, ~~gridded at a 10km~~ resampled at a 10 km resolution. The 18.7 GHz channel is used as it is slightly more sensitive to liquid water content than the ~~others~~ other frequencies (Picard et al.,

2022). Ascending ~~and descending~~ (satellite path goes from south to north) and descending (satellite path goes from north to south) paths were processed separately~~to create two melt masks .~~

~~Melt detection~~ , as they respectively happen in the morning and in the evening. The separated processing allows the creation of two wet-snow masks from one dataset. Wet-snow detection with AMSR2 is based on a change ~~of the snowpack 's~~ in the snowpack physical properties. ~~Dry, the~~ A dry snowpack has a lower emissivity (ϵ) than ~~wet, changing the microwave behaviors in the snowpack (Mätzler, 1987)~~a wet snowpack (Zwally and Fiegles, 1994). For the passive microwave sensors, this ~~change~~ increased emissivity is observed through ~~an~~ augmentation of brightness temperature ~~(Figure 2), caused by the increase in emissivity (Zwally and Fiegles, 1994) :~~

$$TB(\lambda) = \epsilon * TP$$

~~with TB(λ) the wavelength-dependent brightness temperature, and TP the temperature as a physical quantity. The melt~~ (Johnson et al., 2020).

The wet-snow retrieval technique applied for this study is a statistical approach developed by Fahnestock et al. (2002) and modified by Johnson et al. (2020). The ~~melt~~ wet-snow detection is performed through a K-mean clustering algorithm~~(Figure 3)~~. The algorithm is applied to the annual time series of brightness temperature. ~~Melt~~ Wet snow is assumed when the time series ~~show~~ shows a binomial distribution~~. Criterias and thresholds used are the same as in Johnson et al. (2020) to assume the binomial distribution~~, using the criteria and thresholds defined in Johnson et al. (2020) (Figure 2).

~~Evolution of backscattering coefficient σ_0 (in blue) and brightness temperature (orange) over the Larsen C ice shelf (top, 67.54S 63.90W) and the Wilkin coast (bottom, 68.08S 65.86W) over the 2019-2020 melt season. In a place where not melting is observed (top), σ_0 and the brightness temperature shows almost no changes. On the contrary, in areas subject to melt (bottom), we can observe a decrease of σ_0 and an increase in the observed brightness temperature.~~

To ensure coherency between remote sensing products and our climate model, the ~~melt~~ wet-snow masks are interpolated on ~~a common grid. Grids are overlapped and for each MAR pixel , the state of melting is determined by the most dominant melt~~the MAR grid. The grids are superimposed, and the dry/~~no-melt surface~~ wet state for each pixel in the MAR is determined based on the most prevalent wet or dry condition observed in the corresponding area of the satellite mask. This interpolation is made with the hypothesis that the deformations and variations of the area caused by the spatial projection are negligible between a pixel and its neighbors.

~~The radar dataset~~

2.0.2 Sentinel-1

One of the active sensor datasets is retrieved from the Sentinel-1 (S1) ~~satellites~~ satellite constellation from the European Space Agency's (ESA) Copernicus space program. Starting with the launch of S1-A in 2014, the Sentinel-1 constellation gives access to data combining high spatial resolution and lower revisit time covering most of the globe. With the Synthetic Aperture Radar (SAR) technology, S1 products reach a spatial resolution of the order of tens of meters ~~every~~ with a repeat pass of 6 days. By combining different orbital paths, it is possible to reduce the time between two observations of the same location to 2-3 days in

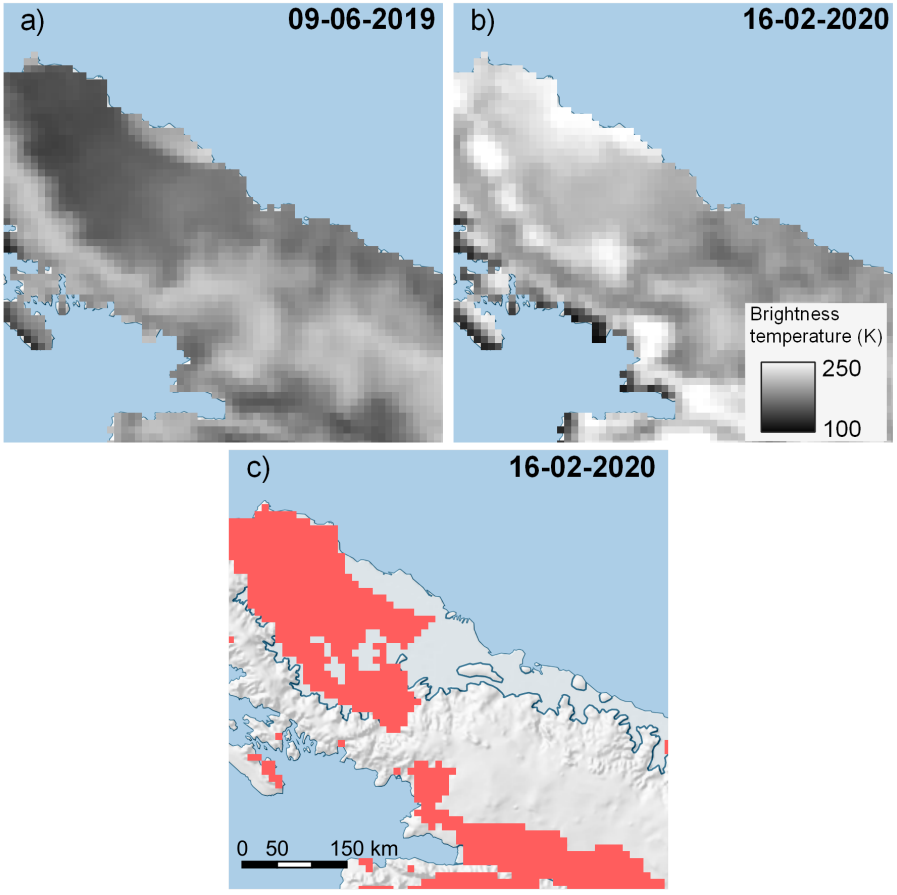

Figure 2. Detection of ~~melt~~ wet snow in an AMSR2 image over the Antarctic Peninsula. (a) Temperature brightness (K) the 09-06-2019. (b) Temperature brightness (K) the 16-02-2020. (c) Pixels considered as wet snow after applying the wet-snow detection algorithm. The increase in ~~TB~~ temperature brightness between (a) and (b) is ~~interpreted as~~ attributed to the presence of liquid water in the snowpack.~~After thresholding, the light red areas are pixels considered as melt.~~

the ~~AP~~Antarctic Peninsula. Working in C-band (5.405 GHz), ~~these SAR sensors can react to~~ it is possible to detect the presence of liquid water in the snowpack ~~with~~ in Sentinel-1 images by identifying changes in backscattering coefficient σ_0 ~~(Figure 4)~~through time (Johnson et al., 2020). With the increase in liquid water in the snowpack, comes a change in absorptivity and ~~in scattering mechanism (Nagler and Rott, 2000; Johnson et al., 2020)~~scattering mechanism (Nagler and Rott, 2000). These two phenomena both lead to a decrease in the observed backscattering coefficient σ_0 (Moreira et al., 2013). As this coefficient changes little in Antarctica as long as the snowpack is dry, it is assumed that a significant change in backscattering is likely caused by the presence of water in the snowpack.

As for the passive sensors, several algorithms have been proposed to detect water in the snow with SAR and active sensors in general. Depending on the polarization, the frequency, and the nature of the snowpack, the threshold applied to the backscatter-

ing values is variable ~~(Winebrenner et al., 1994; Koskinen et al., 1997; Nagler et al., 2016)~~(Koskinen et al., 1997; Nagler et al., 2016) . For a C-band radar, a 3-dB decrease in σ_0 has been employed as a threshold by Nagler and Rott (2000) and Johnson et al. (2020). ~~Later, Liang et al. (2021) proposed~~ In the present article, we used a -2.66 dB threshold after the normalization of the images to their winter mean ~~as the threshold~~ to classify snowpack as dry/wet. This threshold has been proposed by Liang et al. (2021) and was found to be effective on the Antarctic ice sheet.

To minimize the time between two acquisitions of Sentinel-1, all the available images were processed. To handle the quantity of data, image processing was carried out on Google Earth Engine (GEE, Gorelick et al., 2017). The S1 dataset available on GEE is already preprocessed following the implementation of the Sentinel-1 Toolbox from ESA ~~(GEE, 2022; ESA, 2022)~~ (GEE, 2022; ESA, 2022). These processing operations include an update of the orbit metadata, removal of the low-intensity noise on the scene edges, a reduction of the discontinuities between the sub-swath, a radiometric calibration, and a terrain correction from the ASTER digital elevation model. The choice has been made to resample S1 images to a 1 km resolution using mean values before detecting ~~melt. The data will ultimately be~~ wet snow as data is ultimately interpolated on the 7.5 km MAR grid. Before resampling, a 3x3 refined ~~lee speckle~~ Lee speckle low-pass filter developed by Mullissa et al. (2021) was applied to the images in addition to a radiometric terrain flattening using the 1 arc-minute global ETOP1 DEM (Amante and Eakins, 2009). Pixels with values lower than -28 dB were removed from the dataset.

After resampling, the images are normalized to their ~~winter mean, using a technique called "co-orbit normalization" (Liang et al., 2021) or "winter-normalization"~~austral winter mean. The winter mean is ~~calculated with~~ the average value of σ_0 for each pixel, calculated with the observations from June to October. ~~Pixels with values lower than -28 were removed from the dataset.~~ To deal with the changes in volumetric scattering related to the acquisition geometry, ~~even if the images are supposed to be topography-free (terrain-corrected and terrain flattened),~~ only the acquisitions from the same orbit and ~~scene~~ overlapping at more than 95% are taken into account to calculate the winter mean. Consequently, differences between the acquisitions are independent of the topography and the local context. The ~~melt~~ liquid water in the snowpack is then detected in the image by applying the -2.66 dB threshold (Figure ~~4~~3), following Liang et al. (2021).

To create daily ~~images of melt,~~ wet-snow masks, Sentinel-1 images of the same day were combined. In ~~case of overlapping images , the pixel-wise melt~~ the case where three or more images overlap, the snow state is selected by a ~~temporal majority filter. The~~ majority filter, and the acquisition time is defined as the mean time between the selected acquisitions. ~~Else, if~~ In the case where there are only two images that contradict each other, the ~~non-melting~~ non-wet status is assumed. The acquisition time selected is the acquisition time of the non-wet image.

2.0.3 Advanced Scatterometer

The third sensor we are using for this study is the C-band "Advanced Scatterometer" (ASCAT) ~~,~~ aboard the MetOp satellites from the space segment of the EUMETSAT Polar System. ASCAT data are retrieved from the EUMETSAT data service portal (EUMETSAT, 2023). After resolution enhancement (Lindsley and Long, 2016), it provides a backscattering coefficient σ_0 at 4.45~~-km -~~km resolution by accumulating images over about 2 days. In Antarctica, only morning passes are selected for this process. The detection of the ~~melt~~ wet snow uses a simple threshold technique (Ashcraft and Long, 2006)~~. The June-August~~

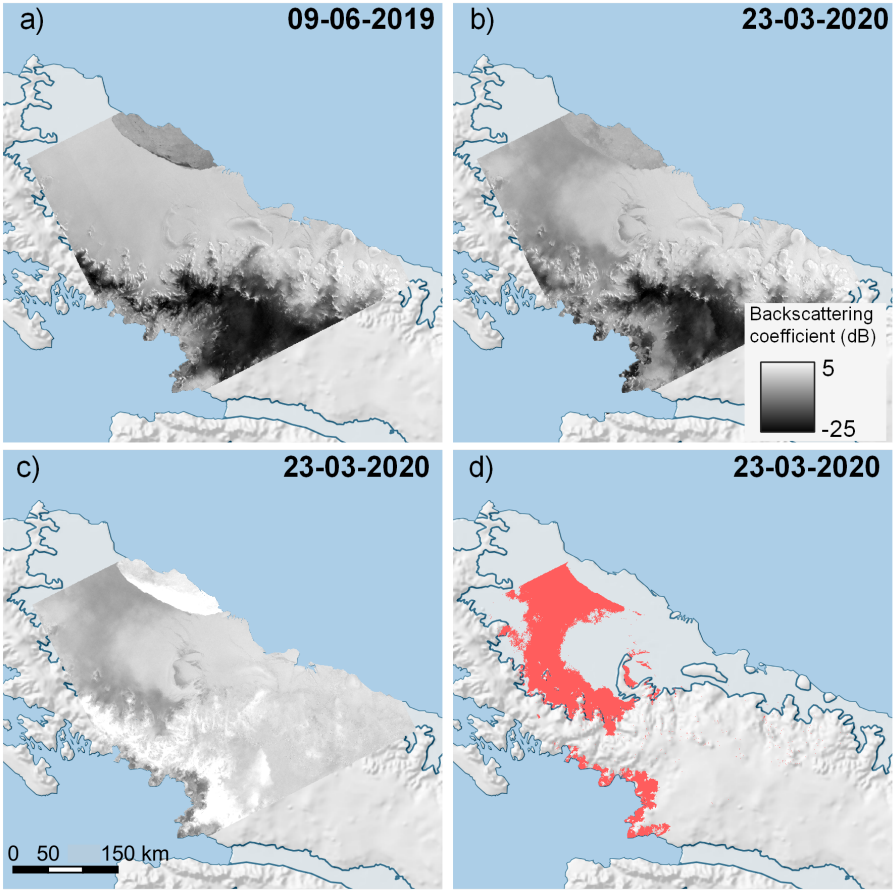

Figure 3. Detection of ~~melt~~ wet snow in a Sentinel-1 image over the Antarctic Peninsula. (a) Backscattering coefficient σ_0 (dB) the 09-06-2019.(b) Backscattering coefficient σ_0 (dB) the 23-03-2020. (c) Normalized backscattering coefficient of the 23-03-2020 to its winter mean. (d) Pixels considered as wet snow after thresholding the normalized image. The decrease in backscatter between (a) and (b) is ~~interpreted as~~ attributed to the presence of liquid water in the snowpack~~. After thresholding, the light red areas are pixels considered as melt.~~

~~mean~~ , similar to the one used for Sentinel- 1 images. The winter-mean backscattering coefficient is first calculated for each pixel and each year ~~, and then~~ from the observations from June-August. Then every measurement lower than this mean -3 dB is considered ~~as melting. Similar~~ wet snow. Similarly to AMSR2 ~~daily products~~daily-products, the Sentinel-1 and ASCAT daily ~~melt~~ wet/dry images are interpolated on the MAR grid. In the end, from the three satellite datasets, four binary masks have been created. One from Sentinel-1, one from ASCAT, and two from AMSR2 by splitting the ascending (evening) and the descending (morning) passes.

2.1 The regional climate model

We employed the Regional Climate Model MAR. MAR is a polar-oriented regional climate model mostly used to study both the Greenland ~~(Delhasse et al., 2020; Fettweis et al., 2021)~~ (Delhasse et al., 2020; Fettweis et al., 2021) and Antarctic ice sheet ~~(Glaude et al., 2020; Amory et al., 2021; Kittel et al., 2021)~~(Glaude et al., 2020; Kittel et al., 2021). Its atmospheric dynamics are based on hydrostatic approximation of primitive equations originally described in Gallée and Schayes (1994) and the radiative transfer scheme is adapted from Morcrette (2002). The transfer of mass and energy between the atmospheric part of the model and the soil is handled by the Soil Ice Snow Vegetation Atmospheric Transfer module (SISVAT, Ridder and Gallée, 1998), from which snow and ice albedo sub-modules are based on CROCUS (Brun et al., 1992). The model has been parameterized to resolve the topmost 20 meters of the snowpack, divided into 30 layers of ~~time varying thickness.~~ time-varying thickness. MAR is configured with a decreasing vertical resolution of the snow layers from the top to the bottom. The first layers are typically at the centimeter size while under the first meter, they are at the meter resolution. The four first maximum layer thicknesses are respectively 2, 5, 10, 30 cm. Each layer has a maximum water content holding capacity of 5 % of its air content beyond which the water freely percolates ~~through the snowpack~~ to the deeper layer or runoffs above impermeable layers (bare ice or ice lenses).

We employed the Regional Climate Model MAR (version 3.12). MAR is a polar-oriented regional climate model mostly used to study both the Greenland (Delhasse et al., 2020; Fettweis et al., 2021) and Antarctic ice sheets (Glaude et al., 2020; Amory et al., 2021; K
. Its atmospheric dynamics are based on hydrostatic approximation of primitive equations originally described in Gallée and Schayes (1994) and the radiative transfer scheme is adapted from Morcrette (2002). The transfer of mass and energy between the atmospheric part of the model and the soil is handled by the Soil Ice Snow Vegetation Atmospheric Transfer module (SISVAT, Ridder and Gallée, 1998) , from which snow and ice albedo sub-modules are based on CROCUS (Brun et al., 1992). The model has been parameterized to resolve the top 20 first meters of the snowpack, divided into 30 layers of time-varying thickness. MAR is configured with a decreasing vertical resolution of the snow layers from the top to the bottom. The first layers are typically at the centimeter size while below the first meter, they are at the meter resolution. The four first maximum layer thicknesses are for example respectively 2, 5, 10 and respectively 30 cm. Each layer has a maximum liquid water content (LWC) of 5 % of its air content beyond which the water freely percolates to the deeper layer or runoffs above impermeable layers (bare ice or ice lenses).

For this work, ~~MARv3.12 was used, including~~ the version 3.12 of MAR was used. It includes recent improvements in the snowpack temperature and the mass water conservation in the soil as described in Lambin et al. (2022). MAR was run at a 7.5 km resolution over the Antarctic Peninsula, with a 40-second time step. It was forced at its lateral boundaries and over ~~ocean~~ the ocean (sea surface temperature and sea ice cover) by the 6-hourly ERA5 reanalysis (Hersbach et al., 2020) between March 2017 and May 2021. ~~Snowpack~~ The snowpack was initialized in March 2017 with a previous MAR simulation (Kittel et al., 2021). ~~Finally, the simulations with assimilation were started in January 2019, restarting from the simulation without assimilation.~~

2.2 Data assimilation

The ~~satellites~~ satellite sensors are sensitive to the presence of liquid water ~~in~~ into the snowpack rather than the physical process of melt~~production~~. The aim of the data assimilation is then to guide or constrain the ~~surface melt production of the model by nudging it to~~ model snowpack LWC by nudging its temperature to induce melt or refreeze to match the observed surface state ~~. Correcting the melt occurrence influences the melt production at the same time. For computational reasons, the assimilation routine is called at each MAR time step only during the melting season, between October and April. Outside of this period, no assimilation is performed. The routine consists in~~ (Figure 4). The assimilation routine involves comparing, pixel by pixel, the model and the ~~satellites melt masks, and warms or cools the snowpack to fit the observations~~satellite wet-snow masks. The satellite ~~acquisition time~~ wet-snow mask pixel is used for the assimilation if the indicated acquisition time is separated by less than 1.5 ~~hour~~ hours from the MAR time. As up to three satellite products are assimilated at the same time, three separate cases have been developed depending on the number of assimilated masks. Each case is called according to the number of acquisitions that ~~is~~ are taken into account in the routine~~(Figure 5).~~ . However, a daily cycle in brightness temperature and thus in wet snow can exist over Antarctica (Picard and Fily, 2006). To take it into account, if there are 3 satellite observations available for a pixel for a single day, an observation of dry snow between two wet-snow observations is considered as a false negative. Consequently, the corresponding pixel from the wet-snow masks is excluded for the day. For computational reasons, the assimilation routine is called at each MAR time step only during the melting season, between October and April. Outside of this period, no assimilation is performed, as very little melting events are expected.

The first case of assimilation represents the situation where a single acquisition is available for ~~the timestep~~ a timestep (case "A" in Figure 4). It is ~~also~~ the most frequent case applied (between 90 and 95 % of the ~~time~~ occurrence depending on the year)~~and the basis for the others~~. This case is inspired by the assimilation performed in Kittel et al. (2022). For the 3 hours around the observation (1.5 h before the observation and 1.5 after, so the model has time to adapt its behavior but the impact remains limited), at each MAR time step, the quantity of liquid water modeled within the pixel is compared to the ~~RS-based~~ satellite-based mask. If the quantity of modeled ~~liquid water~~ LWC into the snowpack is under a certain threshold (α) while the satellite mask indicates ~~melt, first snow layers are heated by 0.15~~ wet snow, the snow layers up to a certain depth (Δ_z) ~~that depends on the sensor wavelength, until the melt threshold is reached. In contrast, if the water quantity~~ are heated by 0.15 °C if the snow layer are colder than 0 °C. On the opposite, if LWC is above the threshold α but no ~~melt~~ wet snow is observed by satellites, the ~~snow~~ snowpack is cooled down by the same rate of 0.15 °C~~by~~ . The process is applied at each MAR time step. However, ~~in both cases,~~ two conditions prevent ~~the assimilation to change~~ change in the MAR snowpack temperature. The first is that if the snow density is above 830 $\mathrm{km\,m^{-3}}$, the layer is considered as ice and the model does not permit liquid water to accumulate into ice. The temperature is then not changed as the ~~threshold would~~ LWC threshold should never be reached. The second condition is the temperature of the snow layers above the Δ_z. If their mean temperature is under -7.5 °C, the MAR snowpack is too cold to ~~have melt in the mode~~ be able to produce meltwater in the model by warming its snowpack, and the satellite observation is ~~discarded~~ignored. This operation is repeated until the α threshold is reached or the observation is out of the time range. The choices for thresholds α and Δ_z are discussed in the two next sections, 2.3.1 and 2.3.2.

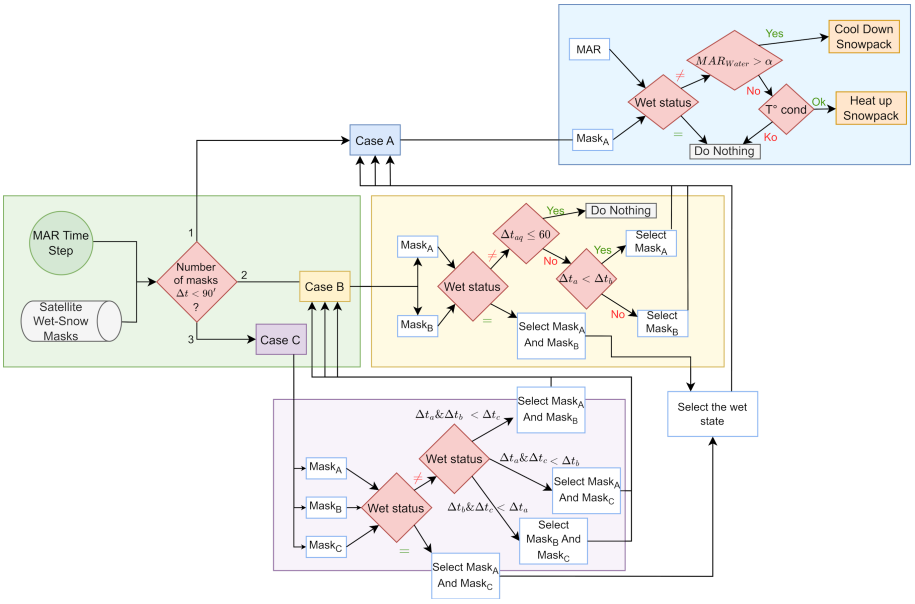

Figure 4. Flowchart of the assimilation algorithm. The number of satellite images available around the MAR time step determines the subprocess that is called in the routine. 3 subprocesses are defined: case A, case B, and case C. They respectively represent the availability of 1, 2, and 3 ~~satellite images~~ wet-snow masks for ~~the~~ assimilation. ~~The cases~~ Cases B and C are funneling to case A so ~~either the images do not give the same~~ no contradictory information ~~and are discarded or multiple acquisition can be interpreted as one~~is given to MAR.

The second case is called when there are two satellite observations at less than 1.5 hours from MAR time (case "B" in Figure 4). If the two masks ~~have the same observation, *i.e.* no melt or melt, the two observations are~~ agree, the two observations are associated with the first case but with a Δ_z equivalent to the mean values of the thresholds that would have been used for individual masks. If the two observations indicate different snow states, a different processing is applied if the acquisitions are close to each other in time (within an hour) or not. For two inconsistent observations spread by more than one hour, the assimilated snow state is the snow state from the closest image to the MAR time, following the first case. For two close contradictory observations, nothing is assimilated as they are considered both equally likely to be correct or wrong. Valuable information may be lost in this case. The difference in penetration depth can cause a deeper penetrating signal to observe liquid water (Figure 5). However, as we have no additional information on the depth at which the water may be present, the model is run as if there was no observation available.

The second case occurs when there are only two satellite observations at less than 1.5 hours from MAR time (case "B" in Figure 4). If the two masks agree, the two observations are associated with the first case but with a depth Δ_z equivalent to the mean values of the thresholds that would have been used for individual ~~observations~~masks. If the two observations indicate different ~~melt~~ snow states, a different processing is applied if the acquisitions are close to each other in time (within an hour) or not. For two inconsistent observations ~~distant~~ spread by more than one hour, the assimilated ~~melt~~ snow state is the ~~melt~~ snow state from the closest image to the MAR time, following the first case (Case "A"). For two close contradictory observations,

nothing is assimilated as they are considered both equally likely to be correct or wrong. ~~The model is thus~~ Valuable information may be lost in this case. The difference in penetration depth can cause a deeper penetrating signal to observe liquid water (Figure 5). However, as we have no additional information on the depth at which the water may be present, the model is run as if there ~~is no observation~~ was no observation available.

The third case is when all three observations are available ~~at the same time~~within the same 3-hour time window (case "C" in Figure 4). As for the second case, if the three masks agree with the same ~~melt~~ wet/non-wet snow status, they are considered as one and ~~as a longer first case~~ the first case is called. Again, the depth Δ_z used is equivalent to the mean values of the ~~threshold~~ thresholds that would have been used ~~otherwise~~separately. If an observation is different from the other two, the two closest observations of the MAR time are analyzed using the second case described here above. For our configuration of sensors, this third case is only encountered a couple of times (less than 1 % of ~~the time) while using~~ all occurrences) while assimilating wet-snow masks of AMSR2 (ascending orbit), ASCAT, and Sentinel-1~~, and so have virtually no implication on the melt estimation~~.

~~Before this case selection, if there are 3 satellite observations available for a pixel for a single day another criterion is applied. Following Picard and Fily (2006) demonstrating a daily cycle in brightness temperature, and thus surface melt, if melt is observed in the earliest and latest observation, an in-between observation with no melt is removed.~~

2.2.1 Choice of water content threshold (α)

2.2.2 ~~Choice of water content threshold α~~

Estimating the quantity of ~~water in~~ liquid water into the snowpack with a single satellite acquisition is challenging. Despite the numerous research studies, the knowledge ~~in~~ on the subject remains limited ~~(Trusel et al., 2013; Fricker et al., 2021)~~ (Trusel et al., 2013; Fricker et al., 2021). However, as described in Picard et al. (2022), it is possible to find a typical water quantity ~~for~~ from which the satellite signal significantly changes ~~,~~ and can be detected as melting~~. Picard et al. (2022) shows that a very small amount of water can be detected with~~ /wet snow. Picard et al. (2022) demonstrates the capability of detecting little amounts of water using the radio frequencies ~~used~~ employed in this study. Only 0.11 and 0.05 ~~are~~ $\mathrm{kg\,m^{-2}}$ of liquid water is necessary at respectively 6 GHz and 19 GHz if the water is uniformly spread over the pixel. This quantity can be higher for heterogeneous pixels containing ~~patches with and without melt~~dry/wet patches. For this study, the choice has been made to use the same threshold no matter the sensor frequency. ~~The passive microwave sensors acquired~~ AMSR2 acquires data at higher frequencies ~~are in principle~~ and is theoretically more sensitive, but ~~having~~ it has a coarser resolution than ~~that of~~ the two active sensors~~, their~~ . Its pixels tend to be more heterogeneous, suggesting a compensation ~~. Two thresholds have been proposed~~ in liquid water quantity. Two different thresholds are tested to study the sensitivity of the model. Both have been shown to significantly change the snowpack brightness temperature in the literature. Tedesco et al. (2007) proposed a LWC threshold of 0.2 % ~~when~~ while Picard et al. (2022) proposed 0.1 % of the snowpack mass being liquid water. They both have already been tested in Kittel et al. (2022) ~~the choice was found to not~~ where the choice between the two was found not to significantly influence the melt quantity produced by the MAR model. The sensitivity of the microwave is high enough that the

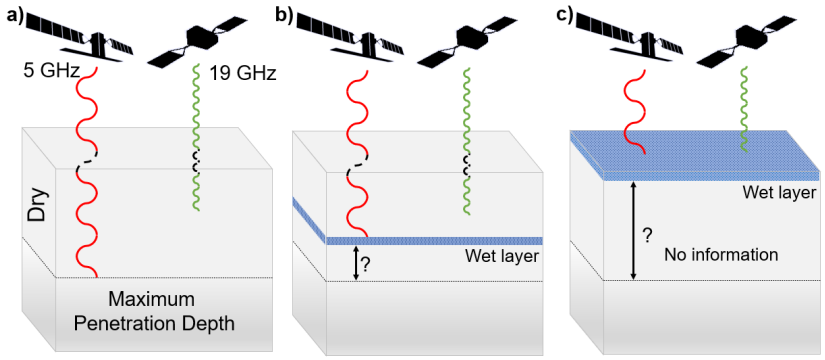

Figure 5. Illustration of the penetration depth of the microwave sensor according to their wavelength and the depth of the wet snow layer. (a) Penetration depth in a dry snowpack. The signal of the sensor with the lower frequency (5 GHz, in red) penetrates deeper than the signal of the higher one (19 GHz, in green). (b) Penetration depth with a layer of liquid water deep in the snowpack. The microwave sensor with deeper penetration ~~is able to~~ can detect ~~melt~~ water presence but the other cannot. (c) Penetration depth with liquid water at the top of the snowpack. Both satellites can observe the presence of liquid water.

quantities of liquid water that can be detected ~~is~~ are much smaller than that produced during a typical melting day ($1.2 \pm 0.6\%$ as modeled by MAR over the studied zone ~~).~~ in the top meter of snow). Currently, there is no clue to identify the best-fitting threshold for this study.

2.2.2 Choice of ~~penetration~~ assimilation depth threshold (Δ_z)

Microwaves have penetration capabilities directly related to their wavelength (Elachi and van Zyl, 2006). As a consequence, C-band ~~SAR~~ from Sentinel-1 and ASCAT has a different penetration depth than Ku-band from AMSR2. In addition, the water content strongly influences the penetration depth, as water at the top of the snowpack can prevent deeper penetration (~~Fig. 6~~Figure 5). In this experiment, we set different ~~limits of penetration for each remote sensing~~ penetration depths for each remote-sensing product to test its influence. Using AMSR2 (Ku-Band), we consider a depth Δ_z = 0.1, 0.2, and 0.4 m successively below the surface. Below this depth, the electromagnetic wave should not have a noticeable influence (Picard et al., 2022). For Sentinel-1 and ASCAT (C-band), the depth ~~threshold~~ thresholds Δ_z ~~is~~ are set up to 0.5, 1, and 1.5 m, as the signal is expected to penetrate deeper in the snowpack.

3 ~~Evaluation~~

2.0.1 Experiences conducted

An ensemble of 24 MAR simulations is presented here. Only the reference MAR simulation, MAR_{ref}, is performed without assimilation. The others are referred to as “assimilations” hereafter. For each one, the satellite wet-snow masks are assimilated

into the model, with different parameters (Table 2). The reference assimilation ($Assim_{ref}$) is using Sentinel-1 and AMSR2, both their ascending and descending orbits, and with thresholds Δ_z = 1 m and 0.2 m respectively. Also, α is set at 0.1 %. The thresholds used to perform $Assim_{ref}$ correspond to values given in the literature (Elachi and van Zyl, 2006; Picard et al., 2022) . The other assimilations have been performed with a combination of 3 satellite products chosen between Sentinel-1, AMSR2 ascending, AMSR2 descending, and ASCAT, and with a combination of the assimilation parameters. The assimilations have been performed from June 2019 to May 2020, and from June 2020 to May 2021.

An ensemble of 24 MAR simulations is presented here (Table 2). Only the reference MAR simulation, MAR_{ref} , is performed without assimilation. The others are referred to as "assimilations" hereafter. Their naming convention is "ASA" followed by the value of α threshold in subscript (in %) and the RS datasets assimilated and their corresponding Δ_z threshold value in subscript (in m). "S1" refers to the S1 dataset, "AMA" to AMSR2 ascending, "AMD" to AMSR2 descending, and "AS" to ASCAT. The assimilations were started in January 2019, and have been restarted from the simulation without assimilation (initialized in 2017). For each one, the satellite wet-snow masks are assimilated into the model, with different parameters (Table 2). The reference assimilation ($Assim_{ref}$) is using Sentinel-1 and AMSR2, both their ascending and descending orbits, and with assimilation depth thresholds Δ_z = 1 m and 0.2 m respectively. Also, the liquid water content threshold α is set at 0.1 %. The thresholds used to perform $Assim_{ref}$ correspond to values given in the literature (Elachi and van Zyl, 2006; Picard et al., 2022) . The other assimilated simulations have been performed with a combination of 3 satellite products chosen between Sentinel-1, AMSR2 ascending, AMSR2 descending, and ASCAT, and with a combination of the assimilation parameters. The present document focuses on the 2019-2020 melt season, while the 2020-2021 season graphs and tables are available in Supplementary Materials.

3 Evaluation

Because the integrated physics within RCMs ~~are~~ is either partially resolved or ~~contain~~ contains uncertainties, it is first required to evaluate ~~models~~ model outputs to in situ measurements. The evaluation is there to quantify how close the model is to reality and if the model is inclined to reproduce this observed situation. Since our focus is on assessing the model sensitivity through assimilation, we exclusively evaluate MAR without assimilation. It is worth noting that the values derived from assimilations may diverge from the observations due to the assimilation algorithm sensitivity rather than the model physics.

The outputs of the non-assimilated model are evaluated by comparing ~~some modeled variables~~ with in situ observations. The daily observations are provided by Automatic Weather Stations (AWS) widespread across the AIS. Here, 9 weather-stations datasets available in the studied zone (blue crosses displayed in ~~Fig.~~ Figure 1) have been gathered to calculate statistics between the model and the observations as done in Kittel (2021) and Mottram et al. (2021). The statistics employed for the evaluation are the Mean Bias (MB), Root Mean Square Error (RMSE), Centered Root Mean Square Error (CRMSE), and correlation (~~Table ??~~r) (Table 3). The statistics are listed for the 2016-2021 period for the ~~near surface~~ near-surface pressure, temperature, wind speed, relative humidity, and modeled energy-balance components, including short-wavelength downward radiations

Table 2. Name of the different simulations and parameterization of the simulation with data assimilation. When not mentioned, both ascending and descending paths of AMSR2 are assimilated. Simulations marked with an asterisk and one sensor assimilation are not taken into account in the calculation of the ensemble average.

Name	α (%)	Ku-band Δ_z (m)	C-band Δ_z (m)	Sensors
$Assim_{ref}$	0.1	0.2	1	AMSR2 + S1
$AsA_{01}S1_{05}AMA_{02}AMD_{02}$	0.1	0.2	0.5	AMSR2 + S1
$AsA_{01}S1_{15}AMA_{02}AMD_{02}$	0.1	0.2	1.5	AMSR2 + S1
$AsA_{02}S1_{10}AMA_{02}AMD_{02}$	0.2	0.2	1	AMSR2 + S1
$AsA_{02}S1_{05}AMA_{02}AMD_{02}$	0.2	0.2	0.5	AMSR2 + S1
$AsA_{02}S1_{15}AMA_{02}AMD_{02}$	0.2	0.2	1.5	AMSR2 + S1
$AsA_{01}S1_{10}AMA_{01}AMD_{01}$	0.1	0.1	1	AMSR2 + S1
$AsA_{01}S1_{05}AMA_{01}AMD_{01}$	0.1	0.1	0.5	AMSR2 + S1
$AsA_{01}S1_{15}AMA_{01}AMD_{01}$	0.1	0.1	1.5	AMSR2 + S1
$AsA_{02}S1_{10}AMA_{01}AMD_{01}*$	0.2	0.1	1	AMSR2 + S1
$AsA_{02}S1_{05}AMA_{01}AMD_{01}*$	0.2	0.1	0.5	AMSR2 + S1
$AsA_{02}S1_{15}AMA_{01}AMD_{01}*$	0.2	0.1	1.5	AMSR2 + S1
$AsA_{01}S1_{10}AMA_{04}AMD_{04}$	0.1	0.4	1	AMSR2 + S1
$AsA_{01}S1_{05}AMA_{04}AMD_{04}$	0.1	0.4	0.5	AMSR2 + S1
$AsA_{01}S1_{15}AMA_{04}AMD_{04}$	0.1	0.4	1.5	AMSR2 + S1
$AsA_{02}S1_{10}AMA_{04}AMD_{04}$	0.2	0.4	1	AMSR2 + S1
$AsA_{02}S1_{05}AMA_{04}AMD_{04}$	0.2	0.4	0.5	AMSR2 + S1
$AsA_{02}S1_{15}AMA_{04}AMD_{04}$	0.2	0.4	1.5	AMSR2 + S1
$AsA_{01}S1_{10}AMA_{02}AS_{02}$	0.1	0.2	1	AMSR2 (asc.) + S1 + ASCAT
$AsA_{01}AMA_{02}$	0.1	0.2	/	AMSR2 (asc.)
$AsA_{01}AMD_{02}$	0.1	0.2	/	AMSR2 (desc.)
$AsA_{01}S1_{10}$	0.1	/	1	S1
$AsA_{01}AS_{10}$	0.1	/	1	ASCAT
MAR_{ref}	/	/	/	None

(SWD), short-wavelength upward radiations (SWU), ~~long-wavelength~~ long- wavelength downward radiations (LWD), and long-wavelength upward radiations (LWU).

Small biases can exist between the in-situ observations and the model due to the elevation difference. The AWS observations are punctual when the model provides zonal information over a 7.5 x 7.5 km^2 pixel. Thus the mean elevation of the MAR pixel in which the AWS falls is not the same as the AWS true elevation. This difference is particularly noticeable for the near-surface pressure, directly linked to the elevation. Nonetheless, a high correlation ($r > 0.98$) reflects the ~~MAR~~ ability to simulate its temporal variability.

Table 3. Mean Bias (MB), Root Mean Square Error (RMSE), Centered Root Mean Square Error (CRMSE), and correlation between MAR and daily observation over the Antarctic Peninsula. A negative value implies a lower MAR estimate than the observation. Statistics are given for the near-surface pressure, temperature, wind speed, relative humidity, shortwave downward (SWD), shortwave upward (SWU), longwave downward (LWD), and longwave upward (LWU) annually, for the summer (DJF), and for the winter (JJA) and are calculated for the 2016-2021 period. During winter, the absence of the Sun implies no short-wavelength solar radiation measurements (SWD and SWU). Locations of the weather station used for the daily observations are marked by blue crosses in Figure 1.

	Annual				Summer				Winter			
	MB	RMSE	CRMSE	Correlation	MB	RMSE	CRMSE	Correlation	MB	RMSE	CRMSE	Correlation
Near Surface Pressure (hPa)	-5.44	14.57	1.25	0.99	-5.69	13.18	0.87	0.99	-6.13	16.09	1.42	0.99
Temperature (°C)	-0.32	3.32	2.81	0.93	-1.13	2.36	1.68	0.76	0.3	3.63	3.11	0.92
Wind speed ($m\,s^{-1}$)	-0.39	2.58	2.28	0.79	-0.43	2.22	1.85	0.7	-0.35	2.92	2.57	0.78
Relative humidity (%)	3.2	8.73	8.13	0.72	6.88	9.32	6.29	0.75	2.87	9.1	8.64	0.79
SWD ($W\,m^{-2}$)	13.87	36.23	33.46	0.97	41.58	59.21	42.15	0.79	/	/	/	/
SWU ($W\,m^{-2}$)	-0.2	24.04	24.04	0.97	14.38	35.81	32.8	0.78	/	/	/	/
LWD ($W\,m^{-2}$)	-14.75	26.15	21.59	0.76	-26.56	32.51	18.75	0.65	-7.12	21.08	19.85	0.81
LWU ($W\,m^{-2}$)	3.4	14.2	13.79	0.93	-0.52	9.2	9.19	0.76	2.83	17.12	16.88	0.9

In general, the winter season is slightly better represented with higher correlations and lower mean bias than the summer season. ~~Larger differences are~~ A weaker correlation is observed in summer for long-wavelength downward radiations ~~LWD~~ ($r = 0.65$). This difference is compensated by the excess of short-wavelength solar radiations ~~over the year. As explained in Delhasse et al. (2020), MAR is outperformed by reanalysis when representing downward radiative fluxes~~in summer. MAR does not assimilate temperature profile nor coastal temperature but is only forced at its lateral boundaries every 6h for its specific humidity and temperature. Thus modeled clouds are the outcome of the model climate and microphysics ~~(Delhasse et al., 2020)~~ Delhasse et al. (2020). Moreover, the radiative scheme implemented in MAR is the one from the ERA-40 reanalysis. This scheme has been updated in the ~~ERA-interim and~~ ERA-5 reanalysis ~~(Hersbach et al., 2018, 2020)~~ (Hersbach et al., 2020) but not in the model. ~~Combined with cloud physics, bias in downward radiative fluxes can appear in MAR.~~ MAR underestimates the liquid water path during summer when compared to Cloudsat-CALISPO estimates described in (Van Tricht et al., 2016). Such underestimation is partially responsible for the LWD bias in summer.

In addition, Jakobs et al. (2020) provide melt estimates from the AWS. These estimates can be compared to the surface melt production of the four closest MAR pixels of the AWS (Figure 6). MAR tends to overestimate some extremes of melting while simultaneously underestimating or overestimating the duration of periods during which the ice shelves are experiencing melting. Even though there can be a difference in altitude between the AWS and MAR pixels that explains the differences between the two datasets, these discrepancies also highlight the importance of nudging MAR to correspond to the remote sensing observation of wet snowpack.

4 Results

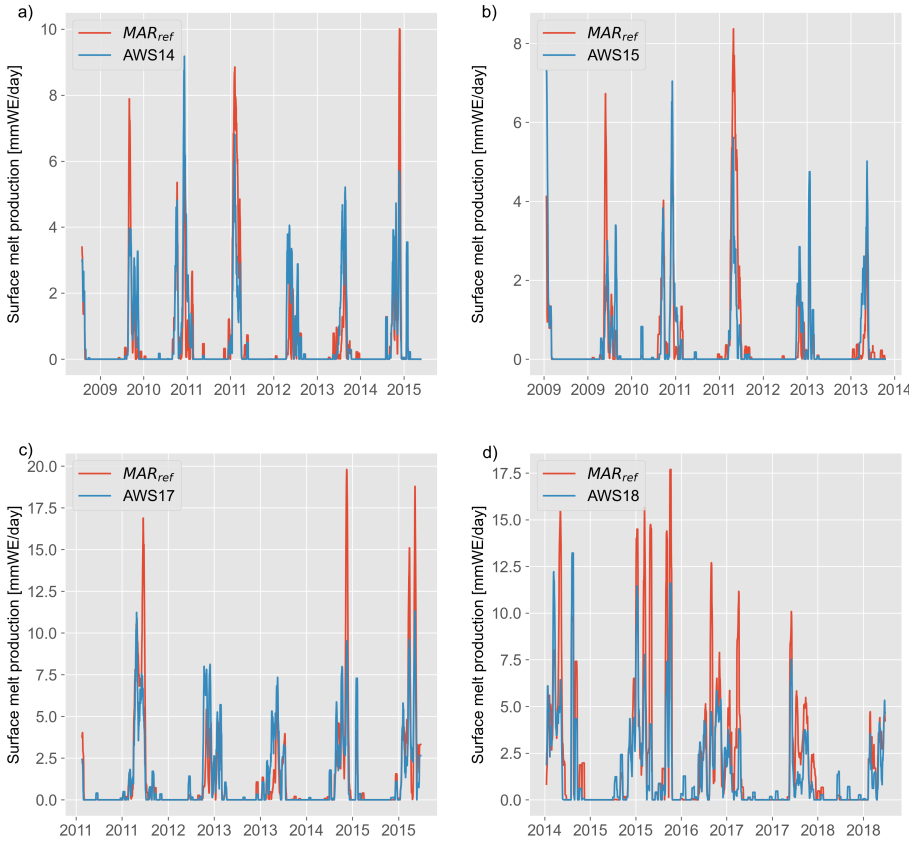

Figure 6. ~~Mean Bias~~ Comparison of surface melt production (~~MB~~mmWEday^{-1}) ~~, Root Mean Square Error~~ as modeled by MAR_{ref} (~~RMSE~~in red) ~~, Centered Root Mean Square Error (CRMSE),~~ and ~~correlation between MAR and daily observation over the Antarctic Peninsula. A negative value implies a lower MAR estimate than the observation. Statistics are given for the for the near~~ estimated surface ~~pressure, temperature, wind speed, relative humidity, shortwave downward~~ melt production from AWS (~~SWD~~a) 14, ~~shortwave upward~~ (~~SWU~~b) 15, ~~longwave downward~~ (~~LWD~~c) 17, and ~~longwave upward~~ (~~LWU~~d) ~~annually, for the summer~~ 18 (~~DJF~~in blue) ~~, and for the winter (JJA) and are calculated for the 2016-2021 period~~described in Jakobs et al. (2020). ~~During winter,~~ In comparison to the ~~absence~~ AWS, MAR tends to overestimate peaks of ~~the Sun implies no short-wavelength solar radiation measurements (SWD and SWU)~~melt but underestimate smaller melt seasons.~~Locations of the weather station used for the daily observations are marked by blue crosses in Fig. 1.~~

~~The results of an ensemble of twenty MAR simulationsis presented here. The reference MAR simulation, MAR_{ref}, is~~ ~~performed without assimilation.~~ Table 4 provides a comprehensive summary of the results obtained from the 24 MAR simulations. The ~~19 others are referred to as "assimilations" hereafter. For each one, the satellite melt masks are assimilated into the model~~summary includes the number of melt days (*i.e.* the number of days where melt is occurring over at least 10 % of the studied zone), surface Melt (ME), Runoff (RU), Refreeze (RZ), and the Surface Mass Balance (SMB). This table offers a concise overview of the simulation results. In the case of assessing the sensitivity of the MAR model to the assimilation, we

analyzed the evolution of several variables (Table 5) including ME, RU, SMB, Snowpack Density (ρ), ~~with different parameters (Table 2) . The reference assimilation ($Assim_{ref}$)is using Sentinel-1~~ and ~~AMSR2, both their ascending and descending orbits, and with thresholds Δ_z = 1 and 0.2 respectively. Also, α is set at 0.1 . The thresholds of~~ Liquid Water Content (LWC) to study the impact caused by the data assimilation. The first 4 variables (ME, RU, RZ, and SMB) are given for the entire snowpack profile while the other two ρ and LWC are given for the first meter. The average value of the variables of all the assimilations, $\overline{Assim}$, is compared to the model with no assimilation. Although $\overline{Assim}$ differs from the reference assimilation, $Assim_{ref}$ ~~correspond to values given in the literature (Elachi and van Zyl, 2006; Picard et al., 2022). The sensitivity tests have been performed from June 2019 to May 2020, and from June 2020 to May 2021. The 2020-2021 season graphs are available in Supplementary materials~~is the closest simulation to $\overline{Assim}$. Three simulations have been discarded to calculate $\overline{Assim}$ because of the unrealistic freeze/thaw cycle induced by the assimilation. These simulations are marked with an asterisk in Table 2. Not to include bias from one wet-snow mask, simulations assimilating only one wet-snow mask are also not used in the calculation of $\overline{Assim}$.

~~The evolution of several variables (Table 3) including surface Melt (ME), Runoff (RU), Surface Mass Balance (SMB), Snowpack Density (ρ), and Liquid Water Content (LWC), is analyzed to study the changes to the model caused by the data assimilation. The first 3 variables (ME, RU, and SMB) are given for the entire snowpack profile while the other two ρ and LWC) are taken at 0.2- and 1-meter depth. The average value of the variables of all the assimilations, $Assim_{mean}$, is compared to the model with no assimilation. Although $Assim_{mean}$ gives different results from the reference assimilation, $Assim_{ref}$ is the closest simulation to $Assim_{mean}$.~~

The surface melt production is larger ~~compared to MAR_{ref}~~ for all assimilations, compared to MAR_{ref}. On average, the ~~melt~~ wet-snow extent provided by the ~~melt masks are~~ wet-snow masks is larger than the ~~melt~~ extent modeled by MAR_{ref} on the Antarctic Peninsula. This difference impacts the melt production in the model~~(Fig. 7).~~. No matter the parametrization of the assimilation, the surface melt production is increased compared to MAR_{ref} (Table 5), leading to ~~an~~ a cumulated melt production increase of ~~63.8~~ 66.7 % for ~~the $Assim_{mean}$~~ $\overline{Assim}$ over the year.

~~Cumulated surface melt production () for the 2019-2020 melt season as modeled by MAR without assimilation (MAR_{ref} in light red), with data assimilation ($Assim_{member}$ in dashed lines), and their averaged value ($Assim_{mean}$ in blue). Shaded areas represent the range of the assimilations.~~

~~The snowpack~~ The meltwater will eventually either refreeze or runoff, depending on the saturation level of the snowpack. The snowpack can saturate, either from excess in meltwater production or from densification. If snowpack ~~liquid water content~~ LWC exceeds 5 % of the firn air content, the excess water starts to trickle and ~~run off. In Antarctica, runoff is driven by the surface melt production and rainfall (Gilbert and Kittel, 2021)~~runoff (irreducible water saturation). The evolution of runoff is thus directly related to the evolution of melt and the snowpack saturation level ~~. Nonetheless, if the relative evolution between $Assim_{mean}$ and MAR_{ref} is the same for~~ (Figure 7). Therefore, the relative increase in surface melt and runoff ~~(+~~is almost similar between $\overline{Assim}$ and MAR_{ref} (66.7% and ~~+~~63.8%~~respectively), it~~ , respectively) but, their absolute increase is not the ~~case in absolute~~ same (+95 Gt y^{-1} and +21 Gt y^{-1}~~). In other words, the snowpack is still able to~~ , respectively).

Table 4. ~~Name~~ Summary of the ~~different simulation and parameterization~~ results of the ~~simulation with data assimilation. Simulations marked with an asterisk have been removed from~~ different experiments conducted for the ~~calculation~~ study. The number of melt days, cumulated surface meltwater, runoff, refreeze, and surface mass balance over the ~~ensemble average~~2019-2020 melt season are provided for each experiment.

Simulation	~~α (~~Number of melt days	ME (Gt yr^{-1})	~~Ku band Δ_z (~~RU (Gt yr^{-1})	~~C-band Δ_z (~~
$Assim_{ref}$	~~0.1~~ 121	~~0.2~~ 214	~~1~~ 56	~~AMSR2~~
~~$MAR_{a01-ku02-c05}$~~ $AsA_{01}S1_{05}AMA_{02}AMD_{02}$	~~0.1~~ 123	~~0.2~~ 214	~~0.5~~ 55	~~AMSR2~~
~~$MAR_{a01-ku02-c15}$~~ $AsA_{01}S1_{15}AMA_{02}AMD_{02}$	~~0.1~~ 121	~~0.2~~ 213	~~1.5~~ 55	~~AMSR2~~
~~$MAR_{a02-ku02-c10}$~~ $AsA_{02}S1_{10}AMA_{02}AMD_{02}$	~~0.2~~ 129	~~0.2~~ 297	~~1~~ 59	~~AMSR2~~
~~$MAR_{a02-ku02-c05}$~~ $AsA_{02}S1_{05}AMA_{02}AMD_{02}$	~~0.2~~ 129	~~0.2~~ 299	~~0.5~~ 58	~~AMSR2~~
~~$MAR_{a02-ku02-c15}$~~ $AsA_{02}S1_{15}AMA_{02}AMD_{02}$	~~0.2~~ 126	~~0.2~~ 298	~~1.5~~ 60	~~AMSR2~~
~~$MAR_{a01-ku01-c10}$~~ $AsA_{01}S1_{10}AMA_{01}AMD_{01}$	~~0.1~~ 122	~~0.1~~ 293	~~1~~ 56	~~AMSR2~~
~~$MAR_{a01-ku01-c05}$~~ $AsA_{01}S1_{05}AMA_{01}AMD_{01}$	~~0.1~~ 123	~~0.1~~ 289	~~0.5~~ 48	~~AMSR2~~
~~$MAR_{a01-ku01-c15}$~~ $AsA_{01}S1_{15}AMA_{01}AMD_{01}$	~~0.1~~ 121	~~0.1~~ 288	~~1.5~~ 51	~~AMSR2~~
~~$MAR_{a02-ku01-c10*}$~~ $AsA_{02}S1_{10}AMA_{01}AMD_{01}$	~~0.2~~ 130	~~0.1~~ 604	~~1~~ 186	~~AMSR2~~
~~$MAR_{a02-ku01-c05*}$~~ $AsA_{02}S1_{05}AMA_{01}AMD_{01}$	~~0.2~~ 131	~~0.1~~ 626	~~0.5~~ 203	~~AMSR2~~
~~$MAR_{a02-ku01-c15*}$~~ $AsA_{02}S1_{15}AMA_{01}AMD_{01}$	~~0.2~~ 126	~~0.1~~ 581	~~1.5~~ 177	~~AMSR2~~
~~$MAR_{a01-ku04-c10}$~~ $AsA_{01}S1_{10}AMA_{04}AMD_{04}$	~~0.1~~ 120	~~0.4~~ 184	~~1~~ 45	~~AMSR2~~
~~$MAR_{a01-ku04-c05}$~~ $AsA_{01}S1_{05}AMA_{04}AMD_{04}$	~~0.1~~ 123	~~0.4~~ 186	~~0.5~~ 47	~~AMSR2~~
~~$MAR_{a01-ku04-c15}$~~ $AsA_{01}S1_{15}AMA_{04}AMD_{04}$	~~0.1~~ 120	~~0.4~~ 183	~~1.5~~ 45	~~AMSR2~~
~~$MAR_{a02-ku04-c10}$~~ $AsA_{02}S1_{10}AMA_{04}AMD_{04}$	~~0.2~~ 127	~~0.4~~ 214	~~1~~ 53	~~AMSR2~~
~~$MAR_{a02-ku04-c05}$~~ $AsA_{02}S1_{05}AMA_{04}AMD_{04}$	~~0.2~~ 129	~~0.4~~ 221	~~0.5~~ 56	~~AMSR2~~
~~$MAR_{a02-ku04-c15}$~~ $AsA_{02}S1_{15}AMA_{04}AMD_{04}$	~~0.2~~ 126	~~0.4~~ 213	~~1.5~~ 52	~~AMSR2~~
~~$MAR_{a01-ku02-c10}$~~ $AsA_{01}S1_{10}AMA_{02}AS_{02}$	~~0.1~~ 122	~~0.2~~ 191	~~1~~ 47	~~AMSR2 (asc.) +~~
$AsA_{01}AMA_{02}$	121	177	48	1
$AsA_{01}AMD_{02}$	120	143	39	1
$AsA_{01}S1_{10}$	119	148	39	1
$AsA_{01}AS_{10}$	121	155	41	1
MAR_{ref}	~~/~~ 123	~~/~~ 142	~~/~~ 32	~~Non~~

The difference between the increase in meltwater production and the increase in runoff corresponds to the increase in refreezing. This suggests that the snowpack can still absorb liquid water ~~as long as it is not fully saturated~~unless it reaches its maximum LWC. The strongest increase in runoff occurs together with firn air content depletion over the ice shelves. Liquid can stay in the porous layers of the surface snowpack. Then, depending on the ~~temperature and the melt production~~available energy in the system, the water either refreezes during the following night or percolates deeper in the snowpack. ~~By~~ But, by

Table 5. ~~Surface~~ Difference (in %) in surface melt production (ME), runoff (RU), refreeze (RZ), surface mass balance (SMB), ~~and average~~ snowpack ~~density (ρ) and snowpack~~ liquid water content (LWC)~~for MAR_{ref}~~, ~~the reference assimilation~~ and snowpack density (~~$Assim_{ref}\rho$~~) between MAR_{ref} and the mean value of the assimilations (~~$Assim_{mean}$~~ $\overline{Assim}$) over the Antarctic Peninsula in 2019 - 2020. Variables are cumulated annually and over summer (from November to the end of April) except for snowpack density and the ~~2019-2020 melt season~~liquid water content which are averaged over the periods. ~~The range comprises all 19 assimilations.~~ LWC and ρ are ~~taken at a depth~~ given as for the average of ~~0.2 and 1~~ the snowpack first meter while the other ~~variable~~ variables are ~~given as a snowpack~~ cumulated ~~value~~on the whole modeled snowpack.

~~Although there are divergences while using different parameters in the assimilation, the~~

	Annual					Summer				
	MAR_{ref}	$Assim_{ref}$	$\overline{Assim}$	Range	Difference (%)	MAR_{ref}	$Assim_{ref}$	$\overline{Assim}$	Range	Difference (%)
ME (Gt yr^{-1})	142	214	237	183 - 299	66.7	140	212	235	180 - 296	67.1
RU (Gt yr^{-1})	32	56	53	45 - 60	63.8	32	56	53	45 - 60	64.5
RZ (Gt yr^{-1})	132	182	206	161 - 258	55.7	128	176	201	157 - 253	56.5
SMB (Gt yr^{-1})	451	427	431	424 - 439	-4.5	253	229	233	226 - 240	-8.2
LWC_{1m} (g kg^{-1})	19	17	18	14 - 24	-6.4	33	29	31	24 - 40	-6
ρ_{1m} (kg m^{-3})	407	422	421	418 - 424	3.6	425	445	445	440 - 449	4.6

refreezing, the water ~~densify~~ densifies the firn, causing firn air content depletion, leaving less storage space for liquid water in the perennial snowpack (Banwell et al., 2021).

As it can be seen in ~~Fig.~~ Figure 8, the data assimilation only has a slight effect on the SMB. The ~~surface mass balance~~ SMB expression is defined as the sum of the ablation terms (runoff ~~, melt,~~ and sublimation) and accumulation terms (~~*e.g.* precipitation and snow transported by the wind~~snowfall and rainfall). The cumulated SMB for the 2019-2020 melt season is only decreased by 4.5 % compared to the model without assimilation. The general trend of SMB remains positive in the studied zone. Only the ice shelves show negative SMB during ~~periods of intense melting (Fig.~~ austral summer (Figure 9).

The density and ~~liquid water content~~ LWC of the snowpack are also impacted by the assimilation. As presented in Table ~~??~~6, on the ice shelves, where most of the surface melt and refreezing occurs, densification ~~has an effect on the deeper liquid water content. Because the snowpack is denser ,~~ affects the LWC. With a denser snowpack, firn air content is reduced and there is less space for liquid water ~~and thus the liquid water quantity~~ to be absorbed. Therefore, despite the increase in surface melt production, the assimilation process eventually led to a decrease in the amount of liquid water retained in the snowpack~~is lower after assimilation.~~ . This reduction occurs due to the assimilations impact on water retention capabilities of the snowpack.

~~For the~~ All three highlighted ice shelves (Larsen C, Wilkins, and ~~Georges VI) , the evolution follows the same general trend as for the global zone but at different speeds (Table ??). The only exception is that even if~~ George VI) are experiencing an increase in surface melt, refreeze, and runoff (Table 6). On Larsen C and Wilkins ice shelves, the increase in runoff is strongly superior to the increase in surface melt production. Larsen C is the ice shelf experiencing the higher increase of melt in absolute and relative (+~~20~~ 21 Gt y^{-1}~~)~~, ~~and consequently runoff~~ *i.e.* +85.7 %) of the three, and its runoff is tripled (+~~5.7~~ 6 Gt y^{-1}~~)~~, ~~both~~ *i.e.* +311.2 %). However, over the year, its liquid water content ~~at 0.2 depth and 1m depth is increasing instead of decreasing~~

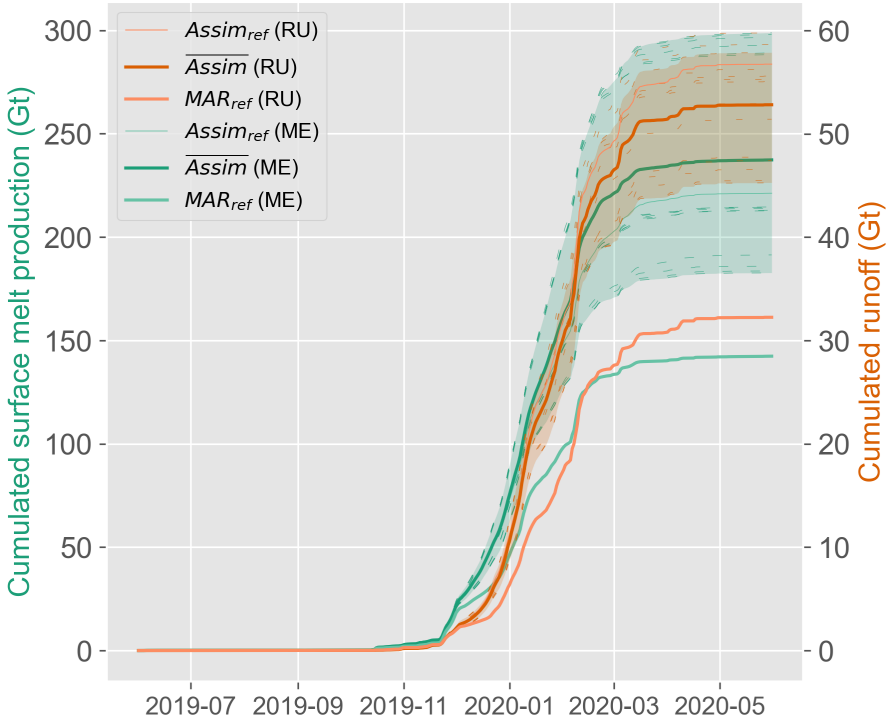

Figure 7. Comparison between the cumulated surface melt (Gt) in green and the cumulated runoff (Gt) in orange for the 2019- 2020 melt season as modeled by MAR without assimilation and with data assimilation. Shaded areas represent the range of the assimilations. While the increase in Gt is larger for melt production, the relative increase is mostly the same for melt production and runoff.

~~(respectively~~ tends to slightly increase (+~~4~~ 1%~~, and~~). It would therefore seem that on ice shelves, the increase in refreezing is not strong enough to compensate for the increase in melting. The depletion of firn air content leads to a swift saturation of the snowpack, making the surplus of meltwater resulting in a more pronounced decrease in SMB compared to other regions of the AP.

All three highlighted ice shelves (Larsen C, Wilkins, and George VI) are experiencing an increase in surface melt, refreeze, and runoff (Table 6). On Larsen C and Wilkins ice shelves, the increase in runoff is strongly superior to the increase in surface melt production. Larsen C is the ice shelf experiencing the higher increase of melt in absolute and relative (+~~12~~ 21 $\mathrm{Gt\,y^{-1}}$, i.e. +85.7 %) of the three, and its runoff is tripled (+6 $\mathrm{Gt\,y^{-1}}$, i.e. +311.2 %). However, over the year, its liquid water content tends to slightly increase (+1 %). It would therefore seem that on ice shelves, the increase in refreezing is not strong enough to compensate for the increase in melting. The depletion of firn air content leads to a swift saturation of the snowpack, making the surplus of meltwater resulting in a more pronounced decrease in SMB compared to other regions of the Antarctic Peninsula.

~~With the exception of the liquid water content, the changes in the snow related variables of the model are so strong that~~ Except for the LWC, which remains relatively small and stable as it has been averaged over the season, the analyzed variables

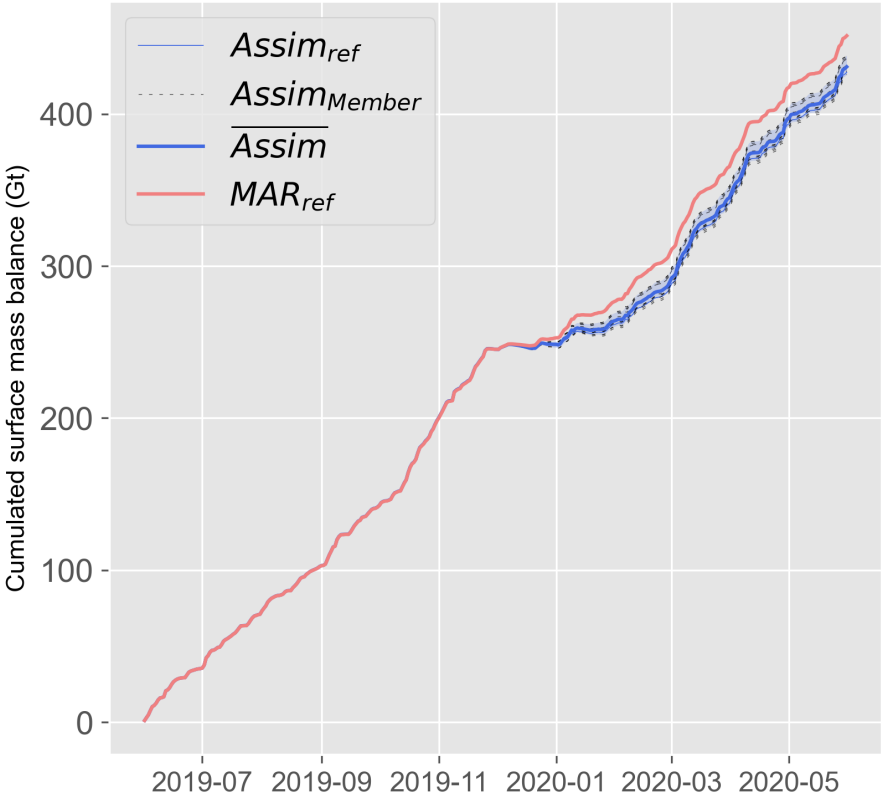

Figure 8. Cumulated surface mass balance (Gt) for 2019-2020 melt season as modeled by MAR without assimilation (MAR_{ref} in red), with data assimilation ($Assim_{member}$ in dashed lines), and their averaged value (~~$Assim_{mean}$~~ $\overline{Assim}$ in blue). Shaded areas represent the range of the assimilations. Despite the increase in surface melt, the surface mass balance does not significantly decrease.

(ME, RU, RZ, SMB, and snowpack density) have undergone noticeable variations, causing MAR_{ref} ~~is out of the range of the different assimilations. The increase in~~ variables to always be outside of the assimilated-simulations range during summer. The amplified surface melt production leads to ~~an increase in the runoffand consequently a decrease in~~ concurrent effects, including increased runoff, reduced surface mass balance~~. The~~ , and an increased occurrence of refreezing. This increase in runoff is ~~explained by the densification of the first~~ attributed to the compaction of the upper layers of the snowpack~~and thus the decrease of its ability to buffer for the~~ , which reduces its capacity to absorb meltwater.

In the end, the results illustrate that, on average, $Assim_{ref}$ is the ~~closest simulation to $Assim_{mean}$,~~ assimilation that gives the closest results to $\overline{Assim}$ and makes it an appropriate candidate when computational resources are limited ~~.~~ (one simulation instead of 24). If the sensitivity to the different parameters of the assimilation is discussed hereafter, the parameters used in $Assim_{ref}$ seem to be an appropriate option.

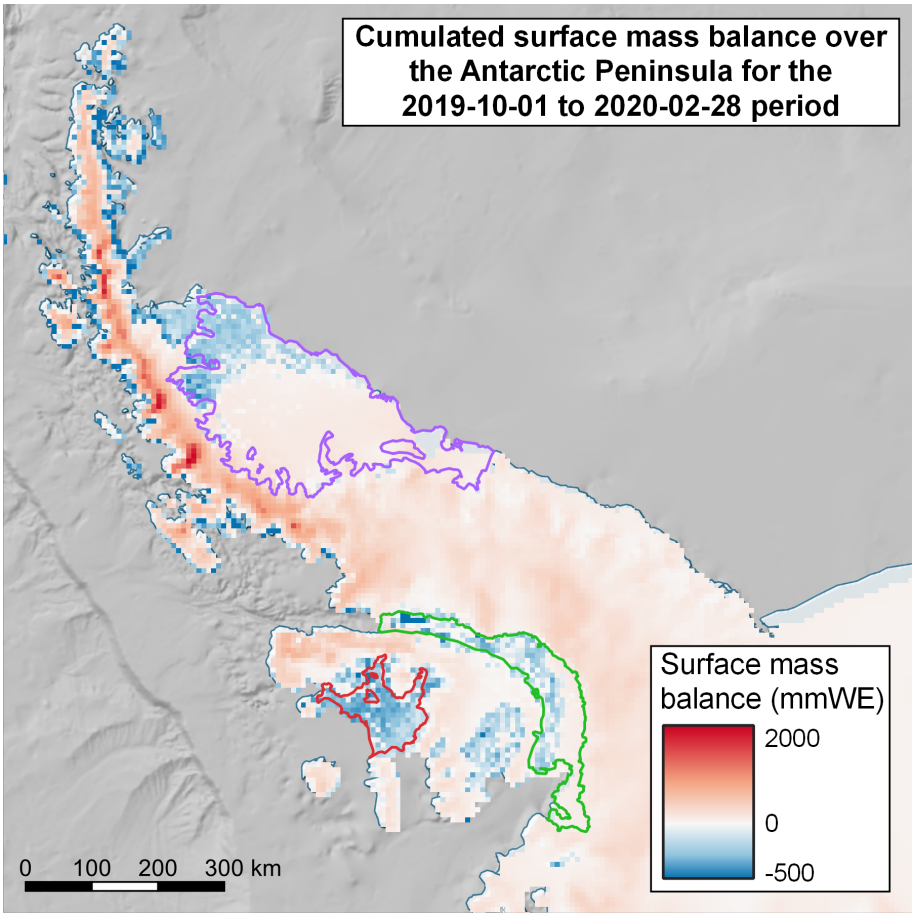

Figure 9. Cumulated SMB (mmWE) from 2019-10-01 to 2020-02-28 over the AP as modeled by $Assim_{ref}$. Larsen C is outlined in purple, ~~Georges~~ George VI in green, and Wilkins in red. The southern ice shelves and the northernmost coastlines are experiencing a ~~decrease in~~ negative SMB in opposition to the rest of the AP. Larsen C is divided in two. Its northern part is experiencing a negative SMB while the southern part is positive.

4.1 ~~Penetration Depth Sensitivity~~The penetration depth MAR sensitivity

4.1.1 Assimilation depth threshold sensitivity

The assimilation depth of low penetrating sensors influences melt production ~~. For the assimilation, we are using a relative liquid water mass in relation to the snowpack weight. Because of the~~ by inducing firn air content depletion. Due to refreezing, the ~~first~~ uppermost 10 centimeters of the snowpack ~~are denser than the first meter. Consequently,~~ becomes denser compared to the top meter. The refereeze is accentuated when using a ~~shallow threshold , the quantity of water required~~ shallow-depth threshold (for example 10 centimeters with AMSR2) as the top layers of the snowpack will contain the majority of the liquid water. Consequently, the increase in melt production to reach the ~~threshold~~ α threshold (0.1% or 0.2%) will be greater ~~as the~~

~~Evolution of surface melt production (ME), runoff (RU), surface mass balance (SMB), snowpack density (ρ), and snowpack liquid water content (LWC) for MAR_{ref}, the reference assimilation ($Assim_{ref}$) and the mean value of the assimilations ($Assim_{mean}$) over the 3 studied ice shelves for the 2019-2020 melt season. LWC and ρ are given at a depth of 0.2 and 1 while the other variable are given as a snowpack average value.~~

Table 6. Difference (%) in surface melt (ME), runoff (RU), refreeze (RZ), surface mass balance (SMB), snowpack liquid water content (LWC), and snowpack density (ρ) between MAR_{ref} and the mean value of the assimilations ($\overline{Assim}$) over the three highlighted ice shelves in 2019 - 2020. Variables are cumulated annually and over summer (from November to the end of April) except for snowpack density and the liquid water content which are averaged over the periods. LWC and ρ are given as for the average of the snowpack first meter while the other variables are cumulated on the whole modeled snowpack.

	Annual					Summer				
Larsen C	MAR_{ref}	$Assim_{ref}$	$\overline{Assim}$	Range	Difference (%)	MAR_{ref}	$Assim_{ref}$	$\overline{Assim}$	Range	Difference (%)
ME (Gt yr^{-1})	23	38	44	31 - 58	85.7	23	38	43	30 - 57	87.6
RU (Gt yr^{-1})	2	7	8	4 - 10	311.2	2	7	8	4 - 10	311.6
RZ (Gt yr^{-1})	22	32	36	28 - 50	62.2	22	31	36	27 - 49	63.6
SMB (Gt yr^{-1})	24	19	18	15 - 21	-25.1	15	10	9	6 - 13	-38.9
LWC_{1m} (g kg^{-1})	3.6	3.5	3.6	3.1 - 4.6	1.5	6.1	6.0	6.2	5.2 - 7.8	1.1
ρ_{1m} (kg m^{-3})	463	508	509	495 - 519	9.8	500	549	552	536 - 564	10.3
Wilkins										
ME (Gt yr^{-1})	9	13	14	10 - 19	48.4	9	12	14	10 - 19	48.2
RU (Gt yr^{-1})	2	5	4	2 - 7	185.6	2	5	4	2 - 7	185.6
RZ (Gt yr^{-1})	9	9	11	9 - 15	22.2	9	8	10	8 - 15	21
SMB (Gt yr^{-1})	6	2	3	0 - 5	-51.3	2	-2	-1	-4 - 1	-141.4
LWC_{1m} (g kg^{-1})	1.3	1.0	1.0	1.0 - 1.21	-21	2.2	1.7	1.7	1.6 - 2.0	-21.2
ρ_{1m} (kg m^{-3})	529	591	578	564 - 597	9.3	599	657	646	626 - 659	7.8
Georges VI										
ME (Gt yr^{-1})	15	20	22	16 - 30	53.2	15	20	22	16 - 30	53.1
RU (Gt yr^{-1})	2	3	3	3 - 4	56.9	2	3	3	3 - 4	56.9
RZ (Gt yr^{-1})	14	18	20	15 - 27	45.8	14	18	20	15 - 27	45.2
SMB (Gt yr^{-1})	11	10	10	9 - 11	-10.3	5	3	3	2 - 4	-25
LWC_{1m} (g kg^{-1})	2.1	1.8	2.0	1.7 - 2.4	-4.1	3.6	3.2	3.5	2.9 - 4.1	-4.1
ρ_{1m} (kg m^{-3})	493	537	526	521 - 537	6.8	544	595	584	577 - 595	7.3

~~densification will eventually cause a heavier snowpack~~than for a deeper assimilation depth where less densification occurs. Also, with firn air content depletion, two other phenomena enhance ~~the~~ melt production. First, the available energy in the system is consumed by ~~refreezing/melting processes, prevailing the snowpack to heat up . A colder snowpack produces less melt and constantly needs larger forcing to reach the melt threshold. Second, because the upper layers are saturated with less water in the bottom layers, the runoff increases~~ the melting process, preventing the layer under 1m from heating up and latent heat from the refreeze process to be released. Therefore, the snowpack will be cooled down by the underneath layers, and will need more nudging. The second point is that during melt events ~~, and the remaining water percolates faster in~~ the ~~deeper~~

~~layers~~upper layers saturate with less water because of the densification. The saturation results in increased runoff and faster percolation of the water into deeper layers, outside of the assimilation depth range. If the model ~~would keep liquid water for a longer time~~ were to retain liquid water in its top snow layers ~~, less melt production would be necessary~~ for a longer duration, it would require less nudging to match the ~~observations~~RS datasets.

This phenomenon is illustrated in ~~Fig.~~ Figure 10, where using a 10 cm assimilation depth threshold for AMSR2 gives ~~double the melt of~~ more melt production than the 20 cm ~~threshold, either~~ and the 40 cm threshold, with both the water content threshold ~~is~~ at 0.1 % or 0.2 %. The effect ends up being so important that using a 10 cm ~~threshold for ASMR~~ assimilation depth and 0.2 % α threshold for AMSR2 can result in ~~improbable results. Consequently, the three simulations with Δ_z = 10 for the Ku-band sensors have been discarded to calculate the average melt for the assimilations. The~~ an intense refreezing and a firn air content depletion that lead to a strong increase in runoff that causes a decrease in SMB for the Antarctic Peninsula. This ~~evolution~~ decrease in SMB is in contradiction with the ~~observed trend that is generally accepted (Rignot et al., 2019; Kittel et al., 2021; Chuter et al., 2022). They were considered outliers and removed from the analysis of the results~~generally observed trend (Rignot et al., 2019; Chuter et al., 2022). Consequently, the three simulations using those parameters for the Ku-band sensors have been discarded to calculate the average melt for the assimilations.

In contrast, with Sentinel-1, the effect of choosing a different Δ_z threshold is less pronounced. As ~~illustrated in Fig. 10, lines with the same color represent~~ shown in Table 4, assimilations that have all parameters in common except the S1 ~~penetration threshold . Almost no variation can be observed between the group of assimilation.~~

assimilation depth threshold only vary by a few $\mathrm{Gt\,yr^{-1}}$ for all variables. Multiple reasons can explain ~~the~~ this comparatively lighter effect. S1 has a ~~much~~ larger revisit time compared to AMSR2 (6 days revisit time vs daily images). With fewer images, the ~~choice of penetration depth is less often considered~~ specific assimilation depth related to S1 is less frequent in the melt assimilation process ~~in~~ within MAR. In addition, as explained previously, the liquid water is kept longer in these slightly deeper layers, and thus no melt is required to reach the water ~~quantity~~ content threshold. The model is thus more sensitive to a shallower ~~penetration~~ assimilation depth threshold. The sensitivity is linked to near-surface events, more likely to occur in the first centimeter of the snowpack. The penetration depth for the C-band sensors is larger than for Ku-band sensors, using sensors with higher frequencies makes the ~~threshold choice~~ choice of the thresholds more sensitive.

4.2 ~~Water content sensitivity~~

4.1.1 Water content threshold sensitivity

The water content sensitivity has a ~~lesser~~ smaller impact compared to the ~~penetration depth. In fact the~~ assimilation depth. The assimilation influences the number of melt days modeled, thus expanding the melt season duration (Table 7) rather than the quantity of liquid water produced by melting. The required amount of liquid water required to reach the ~~thresholds~~ water content thresholds α is small compared to the modeled LWC of a typical melt day. ~~For~~ In MAR_{ref}, for the 2019-2020 melt season, the value reaches 1.2 % for a melt day on average, ~~far~~ above the 0.2 % threshold. ~~Choosing a threshold over the other mostly influences the number of melt days modeled, thus expanding the melt season duration (Table 5) rather than the mass of~~

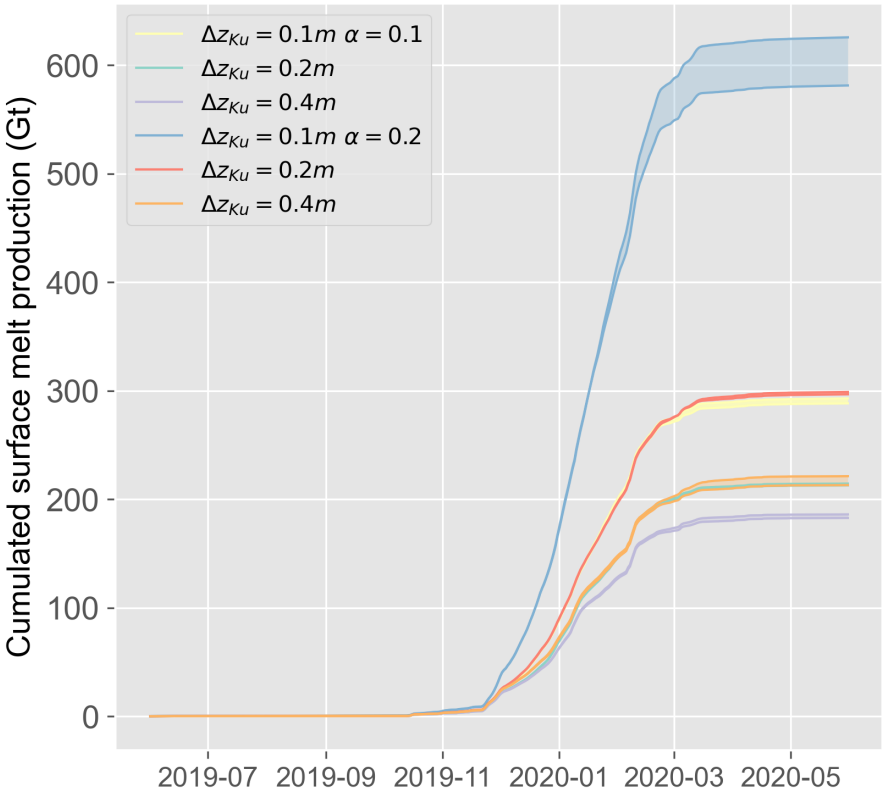

Figure 10. Cumulated surface melt production (Gt) for the 2019-2020 melt season as modeled by the different assimilation. ~~Curves~~ The assimilations are grouped by their α and Ku-band Δ_z thresholds. Shaded areas represent the range of the assimilation of the groups. Groups of assimilations with Ku-band $\Delta_z = 0.1$ m produce more melt than the group of assimilations with the same ~~color have~~ α but different Δ_z ~~for the C-band sensors~~.

~~liquid water produced by melting.~~ For this study, the ~~melt season length~~ number of melt days is defined as the number of days ~~between the first day of the year where more than~~ of the melt season where 10 % of the ice shelf is experiencing melt. ~~The melt season is different from~~ , while the melt season length corresponds to the number of ~~melt days of the ice shelf that is defined as the number of days of the melt season where 10 of the ice shelf is experiencing melt, with~~ days between the first melt day after the first of June and the last melt days before the last day of May of the the following year. Thus, the melt season length also encompasses possible colder periods where no melting event occurs.

~~Using a higher threshold results in an increase in the~~ Choosing a threshold over the other also influences the average number of melt days on the studied ice shelves (~~Fig.~~ Figure 11). ~~The increase in melt days between the 0.1 and 0.2 threshold is caused by the definition of a melt day we used.~~ A pixel is considered as melting for the day if the ~~average~~ daily-averaged mass of liquid water within the first meter of snow is superior to 0.1 % of the snowpack mass. ~~The definition is close to the one used for the assimilation except that the water mass is averaged for the daysrather than taking an instantiate value. Using a higher~~

Table 7. Comparison between the number of days between the first day with observed melt and the last one (the melt season length) and the number of melt days modeled for the three studied ice shelves for MAR_{ref} and the ~~assimilations~~ average number for assimilations depending on their α between June 2019 and May 2020. A melt day over an ice shelf is considered as a day where more than 10 % of the ~~2019-2020~~ ice shelf is experiencing melt~~season~~.

Larsen C	Melt season length (days)	Number of melt days modeled
MAR_{ref}	143	90
$\alpha = 0.1$ %	147	110
$\alpha = 0.2$ %	152	119
Wilkins	**Melt season length (days)**	**Number of melt days modeled**
MAR_{ref}	292	127
$\alpha = 0.1$ %	294	125
$\alpha = 0.2$ %	298	129
~~GeorgesVI~~ GeorgeVI	**Melt season length (days)**	**Number of melt days modeled**
MAR_{ref}	120	120
$\alpha = 0.1$ %	123	122
$\alpha = 0.2$ %	157	134

~~threshold in the assimilation eventually leads to more melt production and thus a higher averaged value for the day.~~ Therefore, using the 0.2 % threshold over 0.1 % will increase the number of melt days.

~~The biggest difference~~ By computing the mean value of each pixel number of melt days of the ice shelves, it was found that the largest deviation occurs on Larsen C~~with an augmentation of the mean number of melt days on the ice shelf by 15 days. For the~~ , with an increase of 15 melt days compared to MAR_{ref}. The other two ice shelves ~~, the differences are smaller with~~ exhibit comparatively smaller differences, with Wilkins and George VI experiencing an increase of 8 and 9 ~~days for Wilkins and Georges VI, respectively . Similar conclusions can be drawn when using 0.2 for the definition of melt days.~~ melt days, respectively (Figure 11).

Taking the assimilation individually leads to a similar conclusion. The water content threshold choice only emphasizes the differences that are caused by the ~~penetration~~ assimilation depth threshold. It is important to note that the simulations that were discarded from the computation of ~~$Assim_{mean}$ are assimilation~~ $\overline{Assim}$ are assimilations that had 0.2 % as the value for the threshold. With a densified snowpack, reaching $\alpha = 0.2$ % required more intense melting.

4.2 ~~Dataset sensitivity~~

4.1.1 Dataset sensitivity

~~The melt datasets used can be highly influential on the results. For a given period, MAR snowpack temperature is forced until a certain level of liquid water in the snowpack is reached in case of a mismatch between the model and the dataset.~~

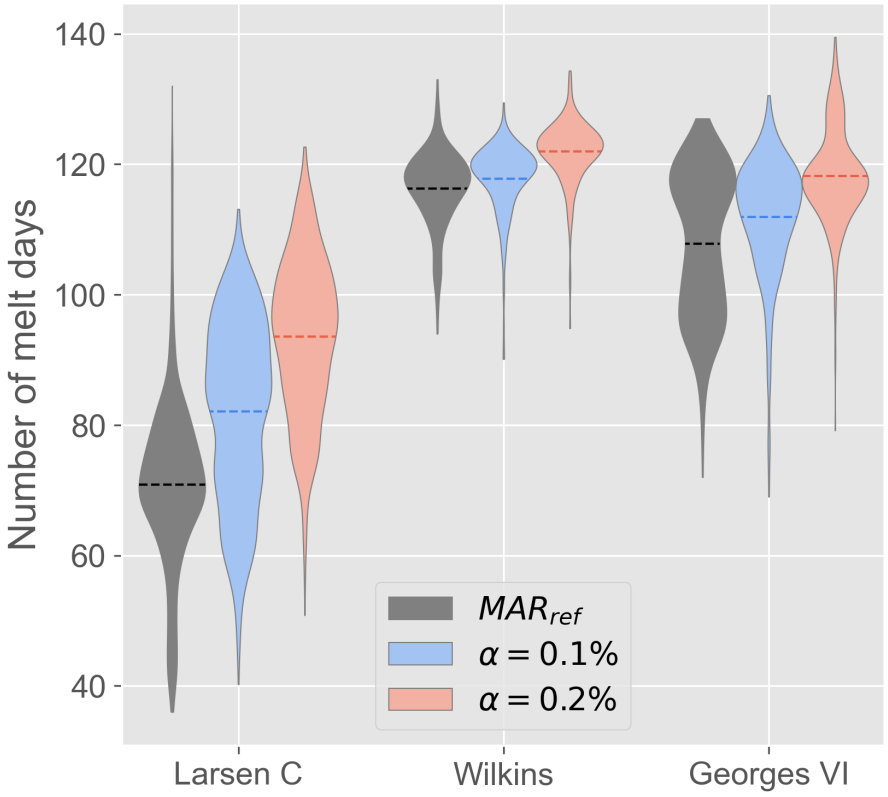

Figure 11. Distribution of the number of melt days ~~fot~~ for the 2019-2020 melt season as modeled by MAR_{ref} and the assimilations ~~for the two~~ grouped by their values of α threshold for the three studied ice shelves. Dashed lines represent the mean value of the distribution. On the three ice shelves, assimilations with α = 0.2 % are experiencing more melt days than MAR_{ref} and the other assimilations. Assimilations with α = 0.2 % are experiencing an increase of the mean number of melt days over the Larsen C ice shelf of 15 days, 8 days on the Wilkins ice shelf, and 9 days on the Georges VI ice shelf.

Each of the four ~~melt masks~~ wet-snow masks (AMSR2 desc., AMSR2 asc., ASCAT, S1) has been assimilated individually into MAR to ~~test~~ study its influence. Assimilating multiple datasets tend to smooth the sensor characteristics as they are only processed to be used where they provide consistent information.

In this study, several characteristics of the remote sensing data have been pinpointed as they influence the results of the assimilation~~. The~~ : the acquisition time, the resolution, and the revisit time. They are discussed hereafter.

First, the acquisition time can artificially lower the number of melt days. Because of the daily cycle of the water quantity in the snowpack, images taken earlier in the morning are less likely to observe ~~melt~~ wet snow (Picard and Fily, 2006). In this manner, over the Antarctic Peninsula, the descending orbit of AMSR2 observes less ~~melt~~ wet snow than the ascending one. Using satellites whose ~~passage~~ acquisition times are well distributed during the day allows them to observe ~~this~~ the daily melt-refreezing cycle and not miss melt days.

Second, the ~~way~~ spatial resolution influences the results of the assimilation ~~is trivial~~because of the pixel heterogeneity. Sensors that have coarser resolution ~~have more heterogeneous pixels and consequently detect melt in places that they should not (and inversely)~~hide a highly heterogeneous surface dynamics and it is possible that while only a fraction of the region covered by one pixel is experiencing melting or enough water is present in the snowpack, the whole pixel is considered as wet snow Picard et al. (2022). In steep regions like near the grounding line, this phenomenon can lead to the detection of wet snow in places where there should not be. In this study, the passive microwave sensor AMSR2 ~~is the only sensor to have~~ has a coarser resolution than ~~the model and whose spatial resolution can be seen in the assimilation results~~MAR and can trigger the assimilation process where it should not.

To study ~~its influence~~ the influence of the spatial resolution, ASCAT has been assimilated (~~$MAR_{a01-ku02-c10}$~~ $AsA_{01}S1_{10}AMA_{02}AS_{02}$ in Table 2) instead of AMSR2 in descending orbit. The ~~two assimilations gave similar~~ assimilations gave smaller numbers of melt days and ~~close~~ surface melt production on the ~~Peninsula ice shelves~~ Antarctic Peninsula for the studied period (191 $\mathrm{Gt\,y^{-1}}$ for ~~$MAR_{a01-ku02-c10}$~~ $AsA_{01}S1_{10}AMA_{02}AS_{02}$ and 214 $\mathrm{Gt\,y^{-1}}$ for $Assim_{ref}$). ~~The major influence for this case~~ If the assimilation depth is different between AMSR2 and ASCAT, the major influence comes from the spatial resolution of the sensor. The difference can be seen on the wet-snow masks (Figure 12). AMSR2 detects melt on Alexander ~~island, between Georges~~ Island, between George VI and Wilkins ice shelves ~~,~~ when ASCAT with a finer resolution and ~~other frequency does not (Fig. 12). With assimilation that uses AMSR2 in ascending and descending orbit, the model ends up melting there. On the contrary, the assimilation taking ASCAT data into account does not force MAR for a long enough time~~ another frequency than AMSR2 does not. Even if wet snow is observed in one of the AMSR masks, the duration of the increased MAR snowpack temperature is too short to produce the water quantities necessary to be detected as a melt day at these places. This preservation of a cold snowpack persists throughout the rest of the day.

Finally, the requirement of the low revisit time is highlighted ~~with the assimilation of Sentinel-1 only . The results of the assimilation are close to the~~ by studying the wet-snow extent resulting from the assimilation of only one sensor at a time (Figure 13). The S1 wet-snow mask assimilated does not cover the entire AP every day and thus shows a smaller wet-snow extent than the other masks. As a consequence, there are fewer instances in which the model and the mask exhibit discrepancies regarding the snow status, resulting in reduced application of the nudging technique. Eventually, S1-only assimilation ($AsA_{01}S1_{10}$ in Table 2) has the closest wet-snow extent to the extent of MAR_{ref} ~~results (Fig. 13).~~ of the assimilation. The resilience of the model ~~is too strong to only use~~ snowpack is such that only relying on a non-daily dataset ~~. The nudgingapplied cannot induce significant changes by being applied every couple of days.Thus,~~ with intermittent nudging, allows it to freely evolve with minimal external forcing.. Consequently, while the high spatial resolution of Sentinel-1 brings valuable information, this advantage is not sufficient enough ~~for it~~ to be used as the only dataset assimilated. ~~However, Sentinel-1 data can~~ The S1 dataset needs to be used in ~~complementarity to~~ conjunction with other datasets to ~~solve the ambiguity problems induced by their spatial resolution~~ combine high spatial resolution with low revisit time.

The resilience of the snowpack also decreases the feasibility of only assimilating one dataset with the algorithm described in this paper. If ASCAT-only assimilation ($AsA_{01}AS_{10}$ in Table 2) tends to be closest to its wet-snow masks, during peaks of

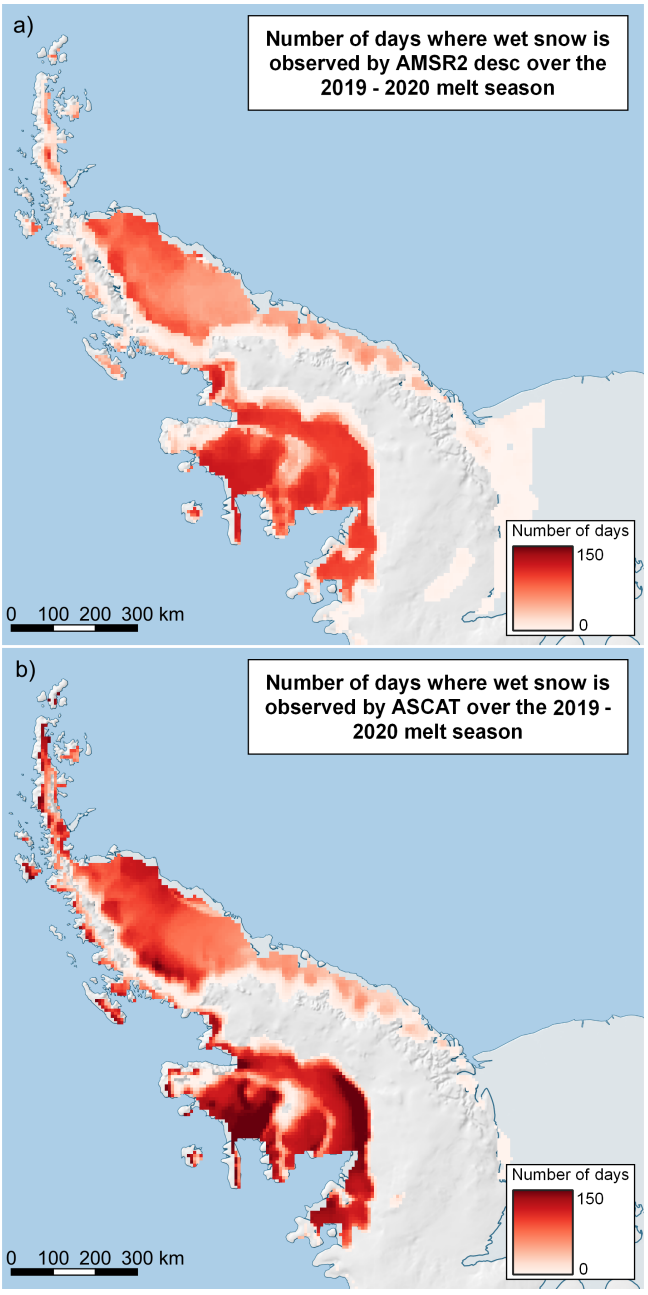

Figure 12. (a) Number of ~~melt~~ days with wet snow observed by AMSR2 ascending on the AP for the 2019-2020 melt season. (b) Number of ~~melt~~ days with wet snows observed by ASCAT on the ~~AP~~ Antarctic Peninsula for the 2019-2020 melt season. ASCAT observes more wet snow than AMSR2 over the ice shelves but less in altitude and slopes on average.

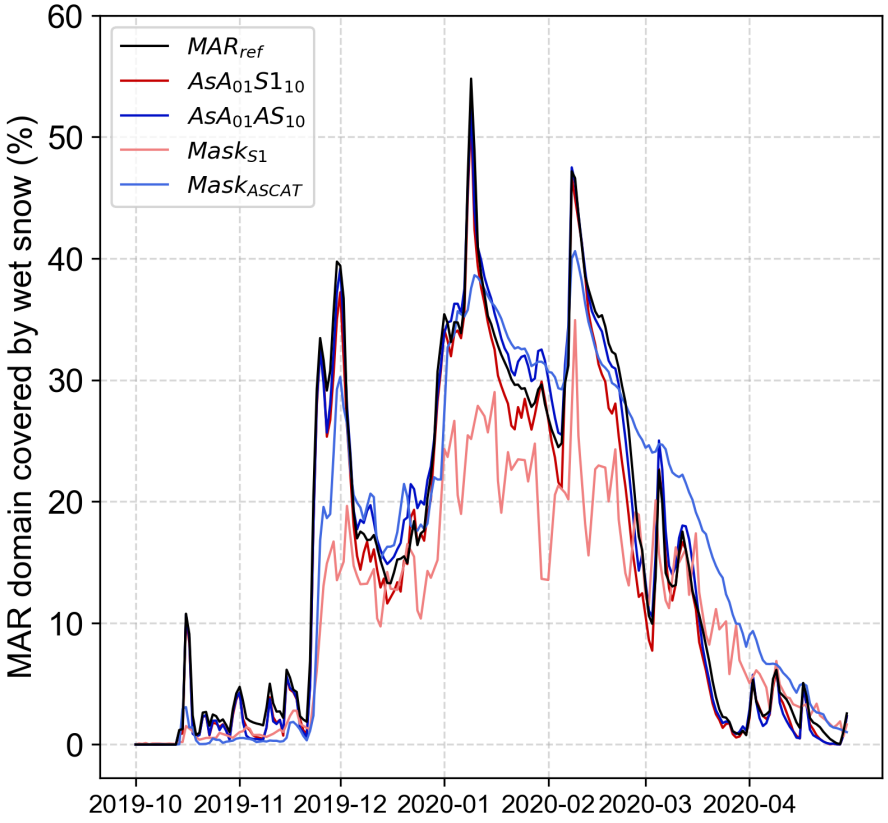

Figure 13. Evolution of the ~~surface melt~~ wet-snow extent during the 2019-2020 melt season as modeled by MAR_{ref} ~~(in light red)~~, ~~$Assim_{mean}$~~ the assimilation of only S1 (~~in blue~~$AsA_{01}S1_{10}$), the assimilation of only ~~S1 melt mask~~ ASCAT (~~$Assim_{S1}$, in green~~$AsA_{01}AS_{10}$), and ~~as observed by AMSR2 in ascending orbit (in grey)~~the wet-snow masks from S1, and ~~by~~ ASCAT~~(in purple)~~. The S1 wet-snow mask has a lower extent as the AP is not covered entirely every day by S1 images.

melt (end of November 2019, beginning of 2020) or strong refreeze (mid-March 2020), the effects of nudging do not persist over long time periods and make the required changes of the model to match the observed wet-snow mask.

~~For now, the restrained period during which the snowpack temperature is modified as well as the possibility not to assimilate~~ Assimilating two datasets that entirely cover the studied zone as well as a dataset that has a finer spatial resolution than MAR serves as a means to mitigate the sensitivity of the model to the chosen datasets. The restrained period in which the model snowpack temperature can be changed and the possibility of not assimilating data in case of discrepancy between the sensors ~~reduce the sensibility to the data set used~~also regulate the dependence of the model on the observations. Future developments ~~of~~ in the technique should allow the ~~inclusion of more datasets during the run~~possibility to assimilate more datasets and weighting wet-snow masks according to the relevance of their wet/dry snow status.

5 Discussion and conclusion

In this paper, we presented the assimilation of ~~surface melt~~ wet-snow occurrence estimated by microwave sensors into the regional climate model MAR. Sensitivity tests have been performed to evaluate the effect of the data assimilation parameters on the model results.

We identified the ~~depth to which the snowpack temperature~~ assimilation depth (Δ_z) ~~as~~ to be the most influential parameter when applied for ~~low penetration~~ shallow-penetration sensors. The influence on the quantity of water produced in the snowpack partially comes from the liquid water content threshold (α) calculation. The ~~very first centimeters~~ uppermost layer of the snowpack ~~are very dense compared to slightly deeper layersbecause of refreezing induced by the liquid meltwater caused by the assimilationand the low temperature at night~~is considerably denser than the underlying layers, owing to the increase in refreezing caused by the exceeding liquid meltwater from assimilation. Heavier and denser layers require more liquid water to reach the required ~~threshold~~ α threshold. Also, the densification causes firn air content depletion, leaving less space for liquid water. ~~Densified, the~~ The densified layer saturates faster, and more runoff occurs.

~~However, the assimilation of surface melt occurrence has a small~~ A threshold of 0.2 m for the Ku-band sensors causes no extreme refreeze or melt and may be considered a good candidate for assimilation depth thresholds. For the C-band sensors, the three thresholds tested yield similar results one or the other, and the implementation of a varying threshold should be considered to take into account the depth at which the wet snow is observed. In contrast to assimilation depth (Δ_z), the LWC threshold (α) has a smaller impact on the ~~atmosphere.~~ model surface melt (in Gt). The choice of α = 0.2 % over α = 0.1 % will mostly increase the duration of the melting season (in number of days).

With constant snowfall (480 G$\mathrm{Gt\,y^{-1}}$) and an increase in the surface melt (+95 $\mathrm{Gt\,y^{-1}}$ or +66.7 %), the increase in runoff (+21 $\mathrm{Gt\,y^{-1}}$ or +63.8 %) translates into a decrease in SMB (-4.5 %), for the 2019-2020 melt season. Nonetheless, runoff values are relatively small compared to the surface mass balance~~. SMB is therefore only slightly affected (-4.5)~~, explaining the small impact on the SMB from the assimilation. The general tendency of SMB remains positive in the studied zone. Only the ice shelves show negative SMB during periods of intense melting.

The assimilated dataset was also found to influence the results of the model after data assimilation. Each sensor has its particularities and ~~melt~~ wet-snow masks may differ from each other. Several of these characteristics have been pinpointed previously. The most important ones are the signal frequency, the revisit time, and the spatial resolution.

The signal frequency of the sensor impacts the resulting melt production by its difference in liquid water sensitivity and the depth to which the signal penetrates. Because it is difficult to provide accurate surface water depth estimates (Fricker et al., 2021) and because microwave signals can be ~~blocked~~ intercepted by the water in the snowpack, the limit at which we stop the assimilation is not always clear. If there is enough water in the top layers, potential liquid water in the deeper layers cannot be observed. In the same way, a thin layer of water can be interpreted as the presence of ~~melt in the~~ water in the first meter of the snowpack when the underneath layers are dry ~~. The~~ (Figure 5). The assimilation depth threshold Δ_z has been set with different values for the different wavelengths of the sensors but remains constant no matter the ~~melting~~ wet state of the snowpack. Introducing a ~~liquid water content~~LWC/density varying threshold could decrease the melt production after the assimilation.

However, we encourage field observation of the evolution of the ~~liquid water present~~ LWC in the snowpack ~~profile would be necessary~~ vertical profile; a required step to introduce and validate ~~such an evolution in~~ the assimilation algorithm.

The revisit time of the satellite is influential as the model ~~is particularly resilient to the nudging of the snowpack temperature~~ freely evolves if the forcing is not performed every day. The assimilation of only Sentinel-1 satellites (revisit time of 6 days, which translates into one image per 2-3 days over the studied zone) is pretty close to the results of the non-assimilated model. Multiple datasets ~~have~~ need to be assimilated during the same day for the model to durably change its behavior. The resilience of the model comes from the refreezing of the snowpack during the night and the winter period. When taking into account a few melt seasons, at the beginning of the melt season, the model snowpack is more or less similar to its previous year state.

Assimilating multiple datasets into MAR ~~does not only have~~ also brings challenges and consideration alongside its advantages. If some missing information is fulfilled by another dataset, it adds another layer of complexity to the algorithm or additional uncertainties linked to the assimilation method used and its thresholds. Datasets may not carry the same information and may not be compatible for all the time steps. Here, none of the datasets is considered to have better ~~melt~~ wet-snow detection than the other. A possible enhancement of the technique would be to add weight to the masks in case of contradiction between them. ~~Weight~~ The weight could be constructed using the confidence level of the ~~melt~~ wet-snow detection technique employed, the satellite spatial resolution, the topography gradient inside the satellite pixels interpolated to the MAR grid ~~,~~ or the sensor sensitivity to water.

The results highlight the importance of data assimilation. While the assimilation does not induce a complete change in the behavior of the model as surface melt remains marginal ~~with respect~~ to snowfall, the snowpack properties tend to deviate from the non-assimilated model impacting ~~at~~ in the end the snowpack's ability to retain future meltwater. Here, satellite data have only been assimilated for two melt seasons over a small area. The study can be conducted for a longer period~~of time~~, at a larger scale or over the Greenland ice sheet where surface melt is the main driver of SMB variability (Slater et al., 2021). Further attention should be given to ice shelves as they are the most sensitive region of Antarctica and important to the Antarctic ice sheet stability ~~(Favier and Pattyn, 2015; Paolo et al., 2015; Sun et al., 2020)~~(Favier and Pattyn, 2015; Paolo et al., 2015; Sun et al., 2020).

Finally, The results obtained in this paper pinpoint the uncertainties of the regional climate model over the ~~AP~~Antarctic Peninsula where, without increasing the snowpack wet extent significantly, the surface melt production significantly increased. The assimilation of remotely sensed data into RCMs is a promising way of reducing the biases and errors inherent to climate models knowing that there is ~~no direct~~ currently no direct large-scale measurement of meltwater content ~~into~~ in the snowpack in Antarctica. This is also an easy way to provide robust uncertainties on model outputs over present climate. Using multiple RS datasets with spatial resolution higher than the one of the model will allow correcting the non-assimilated model by better assessing the snowpack water content.

Code and data availability. The MAR code used in this study is tagged as v3.12 on https://gitlab.com/Mar-Group/MARv3 (MAR model, 2022). Instructions to download the MAR code are provided on https://www.mar.cnrs.fr (MAR Team, 2022). The MAR outputs used in this

study are available upon request by email (tdethinne@uliege.be). Python code and necessary files to perform the assimilation with MAR are available on https://gitlab.uliege.be/tdethinne/assim_mar

Author contributions. TD and XF conceived the study. TD performed the simulations based on a domain of CK. TD led the writing of the manuscript. TD, QG, GP, XF, CK, and AO discussed the results. TD and GP processed the RS data. CK assisted with AWS data comparison. All co-authors revised and contributed to the editing of the manuscript.

Competing interests. The authors declare that they have no conflict of interest.

Acknowledgements. ERA5 reanalysis data (Hersbach et al., 2020) are provided by the European Centre for Medium-Range Weather Forecasts, from their website at https://www.ecmwf.int/en/forecasts/datasets/reanalysis-datasets/era5 (last access: 24 October 2022).

Consortium des Équipements de Calcul Intensif (CÉCI), funded by the Fonds de la Recherche Scientifique de Belgique (F.R.S. – FNRS) under grant no. 2.5020.11 and the Tier-1 supercomputer (Nic5) of the Fédération Wallonie Bruxelles infrastructure funded by the Walloon Region under grant agreement no. 1117545.

Background maps have been provided by the Norwegian Polar Institute through the Quantarctica3 project (Matsuoka et al., 2021).

This project is carried out in the framework of the Digital Twin Antarctica Project European Space Agency ESA Contract [No.4000128611/19/I-DT].

References

Adusumilli, S., Fricker, H. A., Medley, B., Padman, L., and Siegfried, M. R.: Interannual variations in meltwater input to the Southern Ocean from Antarctic ice shelves, Nature Geoscience, 13, 616–620, https://doi.org/10.1038/s41561-020-0616-z, 2020.

Amante, C. and Eakins, B. W.: ETOPO1 arc-minute global relief model : procedures, data sources and analysis. NOAA technical memorandum NESDIS NGDC-24, https://repository.library.noaa.gov/view/noaa/1163, visited on 2022-10-20, 2009.

Amory, C., Kittel, C., Le Toumelin, L., Agosta, C., Delhasse, A., Favier, V., and Fettweis, X.: Performance of MAR (v3.11) in simulating the drifting-snow climate and surface mass balance of Adélie Land, East Antarctica, Geoscientific Model Development, 14, 3487–3510, https://doi.org/10.5194/gmd-14-3487-2021, 2021.

Ashcraft, I. S. and Long, D. G.: Comparison of methods for melt detection over Greenland using active and passive microwave measurements, International Journal of Remote Sensing, 27, 2469–2488, https://doi.org/10.1080/01431160500534465, 2006.

Banwell, A. F., Datta, R. T., Dell, R. L., Moussavi, M., Brucker, L., Picard, G., Shuman, C. A., and Stevens, L. A.: The 32-year record-high surface melt in 2019/2020 on the northern George VI Ice Shelf, Antarctic Peninsula, The Cryosphere, 15, 909–925, https://doi.org/10.5194/tc-15-909-2021, 2021.

Barrand, N. E., Vaughan, D. G., Steiner, N., Tedesco, M., Kuipers Munneke, P., van den Broeke, M. R., and Hosking, J. S.: Trends in Antarctic Peninsula surface melting conditions from observations and regional climate modeling, Journal of Geophysical Research: Earth Surface, 118, 315–330, https://doi.org/10.1029/2012JF002559, 2013.

Bell, R. E., Banwell, A. F., Trusel, L. D., and Kingslake, J.: Antarctic surface hydrology and impacts on ice-sheet mass balance, Nature Climate Change, 8, 1044–1052, https://doi.org/10.1038/s41558-018-0326-3, 2018.

Bouchard, A., Rabier, F., Guidard, V., and Karbou, F.: Enhancements of Satellite Data Assimilation over Antarctica, Monthly Weather Review, 138, 2149 – 2173, https://doi.org/10.1175/2009MWR3071.1, 2010.

Brun, E., David, P., Sudul, M., and Brunot, G.: A numerical model to simulate snow-cover stratigraphy for operational avalanche forecasting, Journal of Glaciology, 38, 13–22, https://doi.org/10.3189/s0022143000009552, 1992.

Church, J., Clark, P., Cazenave, A., Gregory, J., Jevrejeva, S., Levermann, A., Merrifield, M., Milne, G., Nerem, R., Nunn, P., Payne, A., Pfeffer, W., Stammer, D., and Unnikrishnan, A.: Sea Level Change, in: Climate Change 2013: The Physical Science Basis. Contribution of Working Group I to the Fifth Assessment Report of the Intergovernmental Panel on Climate Change, edited by Stocker, T., Qin, D., Plattner, G.-K., Tignor, M., Allen, S., Boschung, J., Nauels, A., Xia, Y., Bex, V., and Midgley, P., Cambridge University Press, Cambridge, United Kingdom and New York, NY, USA., 2013.

Chuter, S. J., Zammit-Mangion, A., Rougier, J., Dawson, G., and Bamber, J. L.: Mass evolution of the Antarctic Peninsula over the last 2 decades from a joint Bayesian inversion, The Cryosphere, 16, 1349–1367, https://doi.org/10.5194/tc-16-1349-2022, 2022.

Colosio, P., Tedesco, M., Ranzi, R., and Fettweis, X.: Surface melting over the Greenland ice sheet derived from enhanced resolution passive microwave brightness temperatures (1979–2019), The Cryosphere, 15, 2623–2646, https://doi.org/10.5194/tc-15-2623-2021, 2021.

Datta, R. T., Tedesco, M., Agosta, C., Fettweis, X., Kuipers Munneke, P., and van den Broeke, M. R.: Melting over the northeast Antarctic Peninsula (1999–2009): evaluation of a high-resolution regional climate model, The Cryosphere, 12, 2901–2922, https://doi.org/10.5194/tc-12-2901-2018, 2018.

Datta, R. T., Tedesco, M., Fettweis, X., Agosta, C., Lhermitte, S., Lenaerts, J. T. M., and Wever, N.: The Effect of Foehn-Induced Surface Melt on Firn Evolution Over the Northeast Antarctic Peninsula, Geophysical Research Letters, 46, 3822–3831, https://doi.org/10.1029/2018GL080845, 2019.

Delhasse, A., Kittel, C., Amory, C., Hofer, S., van As, D., S. Fausto, R., and Fettweis, X.: Brief communication: Evaluation of the near-surface climate in ERA5 over the Greenland Ice Sheet, The Cryosphere, 14, 957–965, https://doi.org/10.5194/tc-14-957-2020, 2020.

Donat-Magnin, M., Jourdain, N. C., Kittel, C., Agosta, C., Amory, C., Gallée, H., Krinner, G., and Chekki, M.: Future surface mass balance and surface melt in the Amundsen sector of the West Antarctic Ice Sheet, The Cryosphere, 15, 571–593, https://doi.org/10.5194/tc-15-571-2021, 2021.

Elachi, C. and van Zyl, J.: Nature and Properties of Electromagnetic Waves, in: Introduction to the Physics and Techniques of Remote Sensing, chap. 2, pp. 23–50, John Wiley and Sons, Ltd, https://doi.org/10.1002/0471783390.ch2, 2006.

ESA: The Sentinel-1 Toolbox, https://sentinel.esa.int/web/sentinel/toolboxes/sentinel-1, visited on 2022-10-19, 2022.

ESA: Sentinel-1 , https://sentinel.esa.int/web/sentinel/missions/sentinel-1, visited on 2023-05-24, 2023.

EUMETSAT: ASCAT Level 1 Sigma0 Full Resolution - Metop - Global, https://navigator.eumetsat.int/product/EO:EUM:DAT:METOP:ASCSZF1B, visited on 2023-05-24, 2023.

Evensen, G.: Data assimilation: The ensemble kalman filter, Springer Berlin, Heidelberg, https://doi.org/10.1007/978-3-642-03711-5, 2009.

Fahnestock, M. A., Abdalati, W., and Shuman, C. A.: Long melt seasons on ice shelves of the Antarctic Peninsula: an analysis using satellite-based microwave emission measurements, Annals of Glaciology, 34, 127–133, https://doi.org/10.3189/172756402781817798, 2002.

Favier, L. and Pattyn, F.: Antarctic ice rise formation, evolution, and stability, Geophysical Research Letters, 42, 4456–4463, https://doi.org/10.1002/2015GL064195, 2015.

Fettweis, X., Tedesco, M., van den Broeke, M., and Ettema, J.: Melting trends over the Greenland ice sheet (1958–2009) from spaceborne microwave data and regional climate models, The Cryosphere, 5, 359–375, https://doi.org/10.5194/tc-5-359-2011, 2011.

Fettweis, X., Hofer, S., Séférian, R., Amory, C., Delhasse, A., Doutreloup, S., Kittel, C., Lang, C., Van Bever, J., Veillon, F., and Irvine, P.: Brief communication: Reduction in the future Greenland ice sheet surface melt with the help of solar geoengineering, The Cryosphere, 15, 3013–3019, https://doi.org/10.5194/tc-15-3013-2021, 2021.

Fretwell, P., Pritchard, H. D., Vaughan, D. G., Bamber, J. L., Barrand, N. E., Bell, R., Bianchi, C., Bingham, R. G., Blankenship, D. D., Casassa, G., Catania, G., Callens, D., Conway, H., Cook, A. J., Corr, H. F. J., Damaske, D., Damm, V., Ferraccioli, F., Forsberg, R., Fujita, S., Gim, Y., Gogineni, P., Griggs, J. A., Hindmarsh, R. C. A., Holmlund, P., Holt, J. W., Jacobel, R. W., Jenkins, A., Jokat, W., Jordan, T., King, E. C., Kohler, J., Krabill, W., Riger-Kusk, M., Langley, K. A., Leitchenkov, G., Leuschen, C., Luyendyk, B. P., Matsuoka, K., Mouginot, J., Nitsche, F. O., Nogi, Y., Nost, O. A., Popov, S. V., Rignot, E., Rippin, D. M., Rivera, A., Roberts, J., Ross, N., Siegert, M. J., Smith, A. M., Steinhage, D., Studinger, M., Sun, B., Tinto, B. K., Welch, B. C., Wilson, D., Young, D. A., Xiangbin, C., and Zirizzotti, A.: Bedmap2: improved ice bed, surface and thickness datasets for Antarctica, The Cryosphere, 7, 375–393, https://doi.org/10.5194/tc-7-375-2013, 2013.

Fricker, H. A., Arndt, P., Brunt, K. M., Datta, R. T., Fair, Z., Jasinski, M. F., Kingslake, J., Magruder, L. A., Moussavi, M., Pope, A., Spergel, J. J., Stoll, J. D., and Wouters, B.: ICESat-2 Meltwater Depth Estimates: Application to Surface Melt on Amery Ice Shelf, East Antarctica, Geophysical Research Letters, 48, e2020GL090 550, https://doi.org/10.1029/2020GL090550, 2021.

Gallée, H. and Schayes, G.: Development of a Three-Dimensional Meso-γ Primitive Equation Model: Katabatic Winds Simulation in the Area of Terra Nova Bay, Antarctica, Monthly Weather Review, 122, 671 – 685, https://doi.org/10.1175/1520-0493(1994)122<0671:DOATDM>2.0.CO;2, 1994.

GEE: Sentinel-1 Algorithms, https://developers.google.com/earth-engine/guides/sentinel1, visited on 2022-10-19, 2022.

Gilbert, E. and Kittel, C.: Surface Melt and Runoff on Antarctic Ice Shelves at 1.5°C, 2°C, and 4°C of Future Warming, Geophysical Research Letters, 48, 9, https://doi.org/10.1029/2020GL091733, 2021.

Glaude, Q., Amory, C., Berger, S., Derauw, D., Pattyn, F., Barbier, C., and Orban, A.: Empirical Removal of Tides and Inverse Barometer Effect on DInSAR From Double DInSAR and a Regional Climate Model, IEEE Journal of Selected Topics in Applied Earth Observations and Remote Sensing, 13, 4085–4094, https://doi.org/10.1109/JSTARS.2020.3008497, 2020.

Gorelick, N., Hancher, M., Dixon, M., Ilyushchenko, S., Thau, D., and Moore, R.: Google Earth Engine: Planetary-scale geospatial analysis for everyone, Remote Sensing of Environment, 202, 18–27, https://doi.org/10.1016/j.rse.2017.06.031, big Remotely Sensed Data: tools, applications and experiences, 2017.

Hersbach, H., Bell, B., Berrisford, P., Biavati, G., Horányi, A., Muñoz Sabater, J., Nicolas, J., Peubey, C., Radu, R., Rozum, I., Schepers, D., Simmons, A., Soci, C., Dee, D., and Thépaut, J.-N.: ERA5 hourly data on single levels from 1979 to present, https://doi.org/10.24381/cds.adbb2d47, visited on 2022-01-22, 2018.

Hersbach, H., Bell, B., Berrisford, P., Hirahara, S., Horányi, A., Muñoz-Sabater, J., Nicolas, J., Peubey, C., Radu, R., Schepers, D., Simmons, A., Soci, C., Abdalla, S., Abellan, X., Balsamo, G., Bechtold, P., Biavati, G., Bidlot, J., Bonavita, M., De Chiara, G., Dahlgren, P., Dee, D., Diamantakis, M., Dragani, R., Flemming, J., Forbes, R., Fuentes, M., Geer, A., Haimberger, L., Healy, S., Hogan, R. J., Hólm, E., Janisková, M., Keeley, S., Laloyaux, P., Lopez, P., Lupu, C., Radnoti, G., de Rosnay, P., Rozum, I., Vamborg, F., Villaume, S., and Thépaut, J.-N.: The ERA5 global reanalysis, Quarterly Journal of the Royal Meteorological Society, 146, 1999–2049, https://doi.org/10.1002/qj.3803, 2020.

Husman, S. D. R., Zhongyang, H., Wouters, B., Munneke, P. K., Veldhuijsen, S., and Lhermitte, S.: Remote Sensing of Surface Melt on Antarctica: Opportunities and Challenges, Journal of selected topics in applied earth observations and remote sensing, https://doi.org/10.1109/JSTARS.2022.3216953, 2022.

Jakobs, C. L., Reijmer, C. H., Smeets, C. J., Trusel, L. D., Berg, W. J. V. D., Broeke, M. R. V. D., and Wessem, J. M. V.: A benchmark dataset of in situ Antarctic surface melt rates and energy balance, Journal of Glaciology, 66, 291–302, https://doi.org/10.1017/jog.2020.6, dataset, 2020.

JAXA: Globe portal system, https://gportal.jaxa.jp/gpr/, visited on 2022-01-10, 2021.

Johnson, A., Fahnestock, M., and Hock, R.: Evaluation of passive microwave melt detection methods on Antarctic Peninsula ice shelves using time series of Sentinel-1 SAR, Remote Sensing of Environment, 250, https://doi.org/10.1016/j.rse.2020.112044, 2020.

Johnson, A., Hock, R., and Fahnestock, M.: Spatial variability and regional trends of Antarctic ice shelf surface melt duration over 1979–2020 derived from passive microwave data, Journal of Glaciology, 68, 533–546, https://doi.org/10.1017/jog.2021.112, 2022.

Kittel, C.: Present and future sensitivity of the Antarctic surface mass balance to oceanic and atmospheric forcings: insights with the regional climate model MAR, Ph.D. thesis, ULiège - Université de Liège, https://hdl.handle.net/2268/258491, 2021.

Kittel, C., Amory, C., Agosta, C., Jourdain, N. C., Hofer, S., Delhasse, A., Doutreloup, S., Huot, P.-V., Lang, C., Fichefet, T., and Fettweis, X.: Diverging future surface mass balance between the Antarctic ice shelves and grounded ice sheet, The Cryosphere, 15, 1215–1236, https://doi.org/10.5194/tc-15-1215-2021, 2021.

Kittel, C., Fettweis, X., Picard, G., and Gourmelen, N.: Assimilation of satellite-derived melt extent increases melt simulated by MAR over the Amundsen sector (West Antarctica), Bulletin de la Société Géographique de Liège, 78, 87–99, https://doi.org/10.25518/0770-7576.6616, 2022.

Koskinen, J., Pulliainen, J., and Hallikainen, M.: The use of ERS-1 SAR data in snow melt monitoring, IEEE Transactions on Geoscience and Remote Sensing, 35, 601–610, https://doi.org/10.1109/36.581975, 1997.

Lai, C.-Y., Kingslake, J., Wearing, M. G., Chen, P.-H. C., Gentine, P., Li, H., Spergel, J. J., and van Wessem, J. M.: Vulnerability of Antarctica's ice shelves to meltwater-driven fracture, Nature, 584, 574–578, https://doi.org/10.1038/s41586-020-2627-8, 2020.

Lambin, C., Fettweis, X., Kittel, C., Fonder, M., and Ernst, D.: Assessment of future wind speed and wind power changes over South Greenland using the Modèle Atmosphérique Régional regional climate model, International Journal of Climatology, pp. 1–17, https://doi.org/10.1002/joc.7795, 2022.

Landmann, J. M., Künsch, H. R., Huss, M., Ogier, C., Kalisch, M., and Farinotti, D.: Assimilating near-real-time mass balance stake readings into a model ensemble using a particle filter, The Cryosphere, 15, 5017–5040, https://doi.org/10.5194/tc-15-5017-2021, 2021.

Liang, D., Guo, H., Zhang, L., Cheng, Y., Zhu, Q., and Liu, X.: Time-series snowmelt detection over the Antarctic using Sentinel-1 SAR images on Google Earth Engine, Remote Sensing of Environment, 256, 112 318, https://doi.org/10.1016/j.rse.2021.112318, 2021.

Lindsley, R. D. and Long, D. G.: Enhanced-Resolution Reconstruction of ASCAT Backscatter Measurements, IEEE Transactions on Geoscience and Remote Sensing, 54, 2589–2601, https://doi.org/10.1109/TGRS.2015.2503762, 2016.

MAR model: MAR, http://www.mar.cnrs.fr, visited on 2022-11-10, 2022.

MAR Team: MARv3.12, https://gitlab.com/Mar-Group/, visited on 2022-11-16, 2022.

Matsuoka, K., Skoglund, A., Roth, G., de Pomereu, J., Griffiths, H., Headland, R., Herried, B., Katsumata, K., Le Brocq, A., Licht, K., Morgan, F., Neff, P. D., Ritz, C., Scheinert, M., Tamura, T., Van de Putte, A., van den Broeke, M., von Deschwanden, A., Deschamps-Berger, C., Van Liefferinge, B., Tronstad, S., and Melvær, Y.: Quantarctica, an integrated mapping environment for Antarctica, the Southern Ocean, and sub-Antarctic islands, Environmental Modelling and Software, 140, https://doi.org/10.1016/j.envsoft.2021.105015, 2021.

Morcrette, J.-J.: Assessment of the ECMWF Model Cloudiness and Surface Radiation Fields at the ARM SGP Site, Monthly Weather Review, 130, 257 – 277, https://doi.org/10.1175/1520-0493(2002)130<0257:AOTEMC>2.0.CO;2, 2002.

Moreira, A., Prats-Iraola, P., Younis, M., Krieger, G., Hajnsek, I., and Papathanassiou, K. P.: A tutorial on synthetic aperture radar, IEEE Geoscience and Remote Sensing Magazine, 1, 6–43, https://doi.org/10.1109/MGRS.2013.2248301, 2013.

Mottram, R., Hansen, N., Kittel, C., van Wessem, J. M., Agosta, C., Amory, C., Boberg, F., van de Berg, W. J., Fettweis, X., Gossart, A., van Lipzig, N. P. M., van Meijgaard, E., Orr, A., Phillips, T., Webster, S., Simonsen, S. B., and Souverijns, N.: What is the surface mass balance of Antarctica? An intercomparison of regional climate model estimates, The Cryosphere, 15, 3751–3784, https://doi.org/10.5194/tc-15-3751-2021, 2021.

Mullissa, A., Vollrath, A., Odongo-Braun, C., Slagter, B., Balling, J., Gou, Y., Gorelick, N., and Reiche, J.: Sentinel-1 SAR Backscatter Analysis Ready Data Preparation in Google Earth Engine, Remote Sensing, 13, https://doi.org/10.3390/rs13101954, 2021.

Mätzler, C.: Applications of the interaction of microwaves with the natural snow cover, Remote Sensing Reviews, 2, 259–387, https://doi.org/10.1080/02757258709532086, 1987.

Nagler, T. and Rott, H.: Retrieval of wet snow by means of multitemporal SAR data, IEEE Transactions on Geoscience and Remote Sensing, 38, 754–765, https://doi.org/10.1109/36.842004, 2000.

Nagler, T., Rott, H., Ripper, E., Bippus, G., and Hetzenecker, M.: Advancements for Snowmelt Monitoring by Means of Sentinel-1 SAR, Remote Sensing, 8, https://doi.org/10.3390/rs8040348, 2016.

Navari, M., Margulis, S. A., Tedesco, M., Fettweis, X., and Alexander, P. M.: Improving Greenland Surface Mass Balance Estimates Through the Assimilation of MODIS Albedo: A Case Study Along the K-Transect, Geophysical Research Letters, 45, 6549–6556, https://doi.org/10.1029/2018GL078448, 2018.

Noël, B., van de Berg, W. J., Lhermitte, S., Wouters, B., Machguth, H., Howat, I., Citterio, M., Moholdt, G., Lenaerts, J. T. M., and van den Broeke, M. R.: A tipping point in refreezing accelerates mass loss of Greenland's glaciers and ice caps, Nature Communications, 8, 14 730, https://doi.org/10.1038/ncomms14730, 2017.

Paolo, F. S., Fricker, H. A., and Padman, L.: Volume loss from Antarctic ice shelves is accelerating, Science, 348, 327–331, https://doi.org/10.1126/science.aaa0940, 2015.

Parkinson, C.: Satellite Passive Microwave Measurements of Sea Ice, in: Encyclopedia of Ocean Sciences, edited by Steele, J. H., pp. 2531–2539, Academic Press, Oxford, https://doi.org/10.1006/rwos.2001.0336, 2001.

Picard, G. and Fily, M.: Surface melting observations in Antarctica by microwave radiometers: Correcting 26-year time series from changes in acquisition hours, Remote Sensing of Environment, 104, 325–336, https://doi.org/10.1016/j.rse.2006.05.010, 2006.

Picard, G., Leduc-Leballeur, M., Banwell, A. F., Brucker, L., and Macelloni, G.: The sensitivity of satellite microwave observations to liquid water in the Antarctic snowpack, The Cryosphere Discussions, 2022, 1–34, https://doi.org/10.5194/tc-2022-85, 2022.

Pollard, D., DeConto, R. M., and Alley, R. B.: Potential Antarctic Ice Sheet retreat driven by hydrofracturing and ice cliff failure, Earth and Planetary Science Letters, 412, 112–121, https://doi.org/10.1016/j.epsl.2014.12.035, 2015.

Ridder, K. D. and Gallée, H.: Land Surface–Induced Regional Climate Change in Southern Israel, Journal of Applied Meteorology, 37, 1470 – 1485, https://doi.org/10.1175/1520-0450(1998)037<1470:LSIRCC>2.0.CO;2, 1998.

Rignot, E., Mouginot, J., Scheuchl, B., van den Broeke, M., van Wessem, M. J., and Morlighem, M.: Four decades of Antarctic Ice Sheet mass balance from 1979–2017, Proceedings of the National Academy of Sciences, 116, 1095–1103, https://doi.org/10.1073/pnas.1812883116, 2019.

Scambos, T., Hulbe, C., and Fahnestock, M.: Climate-Induced Ice Shelf Disintegration in the Antarctic Peninsula, in: Antarctic Peninsula Climate Variability: Historical and Paleoenvironmental Perspectives, pp. 79–92, American Geophysical Union, https://doi.org/10.1029/AR079p0079, 2003.

Slater, T., Shepherd, A., McMillan, M., Leeson, A., Gilbert, L., Muir, A., Munneke, P. K., Noël, B., Fettweis, X., van den Broeke, M., and Briggs, K.: Increased variability in Greenland Ice Sheet runoff from satellite observations, Nature Communications, 12, 6069, https://doi.org/10.1038/s41467-021-26229-4, 2021.

Sun, S., Pattyn, F., Simon, E. G., Albrecht, T., Cornford, S., Calov, R., Dumas, C., Gillet-Chaulet, F., Goelzer, H., Golledge, N. R., and et al.: Antarctic ice sheet response to sudden and sustained ice-shelf collapse (ABUMIP), Journal of Glaciology, 66, 891–904, https://doi.org/10.1017/jog.2020.67, 2020.

Tedesco, M., Abdalati, W., and Zwally, H. J.: Persistent surface snowmelt over Antarctica (1987–2006) from 19.35 GHz brightness temperatures, Geophysical Research Letters, 34, 1–6, https://doi.org/10.1029/2007GL031199, 2007.

The IMBIE Team: Mass balance of the Antarctic Ice Sheet from 1992 to 2017, Nature, 558, 219–222, https://doi.org/10.1038/s41586-018-0179-y, 2018.

Torinesi, O., Fily, M., and Genthon, C.: Variability and Trends of the Summer Melt Period of Antarctic Ice Margins since 1980 from Microwave Sensors, Journal of Climate, 16, 1047 – 1060, https://doi.org/10.1175/1520-0442(2003)016<1047:VATOTS>2.0.CO;2, 2003.

Trusel, L. D., Frey, K. E., Das, S. B., Munneke, P. K., and van den Broeke, M. R.: Satellite-based estimates of Antarctic surface meltwater fluxes, Geophysical Research Letters, 40, 6148–6153, https://doi.org/10.1002/2013GL058138, 2013.

Trusel, L. D., Frey, K. E., Das, S. B., Karnauskas, K. B., Munneke, P. K., Meijgaard, E. V., and Broeke, M. R. V. D.: Divergent trajectories of Antarctic surface melt under two twenty-first-century climate scenarios, Nature Geoscience, 8, 927–932, https://doi.org/10.1038/ngeo2563, 2015.

Van Tricht, K., Lhermitte, S., Lenaerts, J. T. M., Gorodetskaya, I. V., L'Ecuyer, T. S., Noël, B., van den Broeke, M. R., Turner, D. D., and van Lipzig, N. P. M.: Clouds enhance Greenland ice sheet meltwater runoff, Nature Communications, 7, 10 266, https://doi.org/10.1038/ncomms10266, 2016.

Wille, J. D., Favier, V., Jourdain, N. C., Kittel, C., Turton, J. V., Agosta, C., Gorodetskaya, I. V., Picard, G., Codron, F., Santos, C. L.-D., Amory, C., Fettweis, X., Blanchet, J., Jomelli, V., and Berchet, A.: Intense atmospheric rivers can weaken ice shelf stability at the Antarctic Peninsula, Communications Earth & Environment, 3, 90, https://doi.org/10.1038/s43247-022-00422-9, 2022.

Winebrenner, D. P., Nelson, E. D., Colony, R., and West, R. D.: Observation of melt onset on multiyear Arctic sea ice using the ERS 1 synthetic aperture radar, Journal of Geophysical Research: Oceans, 99, 22 425–22 441, https://doi.org/10.1029/94JC01268, 1994.

Zwally, H. J. and Fiegles, S.: Extent and duration of Antarctic surface melting, Journal of Glaciology, 40, 463–475, https://doi.org/10.3189/s0022143000012338, 1994.